SSC-152

TEMPERATURE DISTRIBUTION AND THERMAL STRESSES

BY

P. T. LYMAN and J. L. MERIAM

SHIP STRUCTURE COMMITTEE

SHIP STRUCTURE COMMITTEE

MEMBER AGENCIES:
BUREAU OF SHIPS, DEPT. OF NAVY
MILITARY SEA TRANSPORTATION SERVICE, DEPT. OF NAVY
UNITED STATES COAST GUARD, TREASURY DEPT.
MARITIME ADMINISTRATION, DEPT. OF COMMERCE
AMERICAN BUREAU OF SHIPPING

ADDRESS CORRESPONDENCE TO:
SECRETARY
SHIP STRUCTURE COMMITTEE
U. S. COAST GUARD HEADQUARTERS
WASHINGTON 25, D. C.

June 1964

Dear Sir:

In order to determine the thermal stresses on ships, the Ship Structure Committee has sponsored theoretical and experimental work on the subject. Herewith is the Final Report, SSC-152, Temperature Distribution and Thermal Stresses, by P. T. Lyman and J. L. Meriam.

The project has been conducted under the advisory guidance of the Ship Hull Research Committee of the National Academy of Sciences-National Research Council.

Comments on this report would be welcomed and should be addressed to the Secretary, Ship Structure Committee.

Yours sincerely,

T. J. FABIK
Rear Admiral, U. S. Coast Guard
Chairman, Ship Structure
Committee

SSC-152

Final Report
of

Project SR-161
"Temp. Dist. & Thermal Stress"

to the

Ship Structure Committee

TEMPERATURE DISTRIBUTION AND THERMAL STRESSES

by

P. T. Lyman and J. L. Meriam

University of California
Berkeley

under

Department of the Navy
Bureau of Ships Contract NObs-78634

Washington, D. C.
National Academy of Sciences-National Research Council
June 1964

ABSTRACT

The purpose of the investigation was to extend the existing knowledge of thermal stresses in ship structures by the study of both physical and mathematical models. The physical floating model was a 10-ft welded box beam simulating the main hull girder of a transversely framed cargo ship. It was subjected to various temperature environments above water, and thermal stresses were measured with foil strain gages. The results of these tests showed excellent agreement at sections remote from the ends of the model with a strength-of-materials approach modified to include any arbitrary transverse temperature distribution. Attempts to measure the effect of longitudinal temperature gradients were unsuccessful because of the difficulty of temperature control and the need for more extensive temperature and strain mapping than that which could be undertaken.

A finite-difference solution to the governing equations of thermo-elasticity was developed for two-dimensional plates and extended to a folded-plate type of box girder. The solution was conducted on the IBM 704 and 7090 computers, and the computer program with slight modification is considered suitable for use in ship-design offices. Solutions were obtained for a variety of thermal conditions with temperatures varying vertically, transversely, and longitudinally. Accurate comparisons were made with both the experimental and the strength-of-materials results.

CONTENTS

NATIONAL ACADEMY OF SCIENCES-NATIONAL RESEARCH COUNCIL

Division of Engineering & Industrial Research

SR-161 Project Advisory Committee
"Temp. Dist. & Thermal Stress"

Chairman:

Professor William Prager
Brown University

Members:

Professor B.A. Boley
Columbia University

Mr. John P. Comstock
(Retired)

Mr. Samuel Levy
General Electric Co.

Mr. R. H. Rogers
Esso Tankers, Inc.

INTRODUCTION

The project described in this report was a direct outgrowth of studies conducted on the SS Boulder Victory[1] in 1958. These studies, in turn, were prompted by measurements made on the Esso Ashville in 1955 and reported by N. H. Jasper[2] which indicated the presence of deck stress increments of as much as 10,900 psi attributed to the diurnal transit of the sun. The SS Boulder Victory tests were sponsored jointly by the Society of Naval Architects and Marine Engineers and the United States Maritime Administration. The main objective of this program was to provide a limited but reliable number of temperature and corresponding stress distributions over a complete transverse section of a ship under measurable and partially controlled conditions. To this end, the United States Maritime Administration made available the SS Boulder Victory from the reserve fleet. The SS Boulder Victory was moved to the United States Maritime Administration shipyard at Richmond, California, where a complete transverse section was instrumented for strain and temperature measurements. The results of several series of tests showed very good agreement between the measured stresses and the stresses computed from temperature measurements by the method used by Jasper[2]. These results were the first complete set of full-scale measurements which could be used for comparison with theory. However, these tests were designed to measure mainly the stresses around one complete transverse section of the ship, and were thus limited in scope. The SS Boulder Victory tests showed surprisingly good agreement between measured values of stress and values calculated by modified beam theory for the one section studied. Guided by these results it was felt that a more complete stress-temperature picture of the hull girder was desirable in order to provide information needed for a more rational approach to ship design to account for thermal stresses. Consequently the study reported herein was undertaken through the sponsorship of the Ship Structure Committee.

The purpose of the project was to extend the existing knowledge of thermal stresses in ships by means of experimental measurements on a structural model simulating the hull girder of a transversely framed cargo vessel and by means of theoretical calculations which would extend the beam-theory approach to a more accurate treatment of hull geometry and temperature distribution. To carry out this purpose a model facility was developed for inducing thermal gradients on a 10-ft floating structural model and for measuring the corresponding thermal stresses. Concurrently, a theoretical approach based on elasticity theory was developed and applied to a box girder having length, width, and depth ratios comparable to those of the structural model. Solution of the resulting field equations was accomplished by the development of a computer program.

EXPERIMENTAL

General. The main purpose of the experimental phase of this work was to obtain reliable information on the distribution of thermal stresses in a ship-type structure against which analytical predictions may be compared. A second purpose of the experimental phase was to provide recommendations which may aid in future experimental investigations of thermal stresses in ship-type structures.

To carry out the above objectives, an experimental facility was built which consists of an instrumented model, a water tank for support, a heating system for producing thermal gradients, and the necessary instrumentation. The water tank serves two functions. First, it provides realistic support for the ship model, and second, it provides an adequate heat sink which is necessary in order to maintain the required thermal gradients in the model. The heating system consists of a closed circuit forced-air convection system, with the heat input supplied by steam coils and auxiliary electric heating elements. The air flow was ducted to a hood over the model, then distributed by baffles within the hood over the model, and thence back to the fan and heaters. The water was maintained at a constant temperature by permitting a steady inflow of cold water while maintaining a constant water level with the aid of a weir. The tank and elements of the air heating system are shown in Figures 1 and 2. One-half of the hood may be seen in the background of Figure 2.

Model Design. The correct similitude relationships between model and prototype, considered as beams, are first established. The steady-state thermal stresses in a beam may be represented as a function of the following form:

$$\sigma = f[\alpha, T, E, G, A, I, \ell, x, y, z, --] \quad (1)$$

where the symbols have been defined under nomenclature. If E, ℓ, and T are selected as a basic set of units, the functional relationship may be written using the Buckingham Pi Theorem as

$$\frac{\sigma}{E} = f\left[\alpha T, \frac{G}{E}, \frac{A}{\ell^2}, \frac{I}{\ell^4}, \frac{x}{\ell}, \frac{y}{\ell}, \frac{z}{\ell} \text{ ---}\right] \quad (2)$$

It is clear from this result that if a model is built of the same material, and with the same geometry as the prototype, that the thermal stresses will be equal if the temperature distributions are equal.

In two-dimensional structures it can easily be shown that the thickness of the structure need not be scaled in proportion to the other dimensions. To show this, consider the well known two-dimensional elastic stress-strain law

$$\sigma_1 = \frac{E}{1-\nu^2}[\bar{e}_1 + \nu \bar{e}_2] - \frac{E\alpha T}{1-\nu} \quad (3)$$

where σ_1 = the stress in the 1-direction

$\bar{e}_1$ = the total strain in the 1-direction

$\bar{e}_2$ = the total strain in the 2-direction

ν = Poisson's ratio

and the remainder of the symbols have been previously defined. If the components e_1 and e_2 of strain due only to the induced stresses are measured then:

$$\bar{e}_1 = e_1 + \alpha T \text{ and } \bar{e}_2 = e_2 + \alpha T \quad (4)$$

Upon substituion, the stress-strain law now becomes

$$\sigma_1 = \frac{E}{1-\nu^2}[e_1 + \nu e_2] \quad (5)$$

If the subscripts m and p are used to designate the model and prototype respectively, then

$$\sigma_{1p} = \sigma_{1m} \frac{[E_p/(1-\nu_p^2)]\ [e_{1p} + \nu_p e_{2p}]}{[E_m/(1-\nu_m^2)]\ [e_{1m} + \nu_m e_{2m}]} \quad (6)$$

If the model and the prototype are of the same material, then

$$\sigma_{1p} = \sigma_{1m} \frac{[e_{1p} + \nu e_{2p}]}{[e_{1m} + \nu e_{2m}]} \quad (7)$$

The strain distributions in the model and the prototype are similar if the temperature distributions are similar. Under these conditions, then, the stress distributions will be similar. This result is independent of thickness, and if the same temperature excitation is applied to the prototype and the model, the stresses will be equal.

An experimental model may be used either to predict prototype behavior through accurate scaling, to verify a theory through the check with experimental results, or to aid in the development of analytical and experimental methods. The present model was designed with all three of these purposes in mind, and therefore incorporated a number of compromises. Clearly, exact scaling was out of the question. Nevertheless, it was felt that the basic characteristics of the primary structure of the model could be simulated with a relatively simple structural model. It was intended that structural similarity with the prototype would be maintained close enough so that any valid comparison between proposed design theory and model results would also carry over to the prototype structure to an acceptable degree.

The model used in this investigation was designed to the following requirements:

1. The basic geometry of the midship section should be as simple as possible, consistent with the requirements of the model laws and fabrication techniques.

2. The model should be large enough to permit access to the interior to provide instrumentation, inspection and repair or modification as required.

3. The model cost must be kept to within reasonable budget limitations.

4. Provisions should be made in the design to permit future modifications without having to build a new model.

It was decided to omit certain geometrical features such as 'tween-decks, hatch openings, double bottoms, variations in plate thickness, turn-of-the-bilge, and tapered end sections. While it can be argued that all these features are in the actual ship, and hence required for

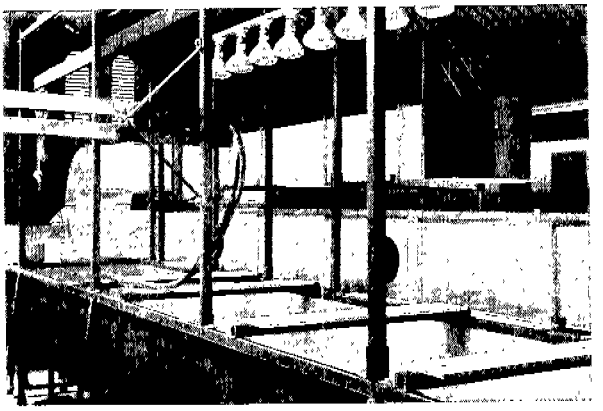

FIG. 1. VIEW OF MODEL TANK.

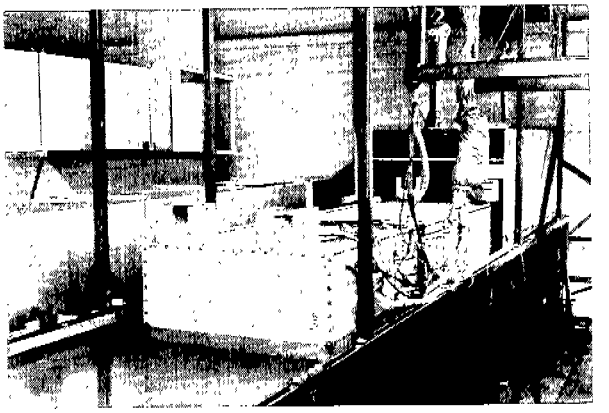

FIG. 2. VIEW OF TANK AND MODEL.

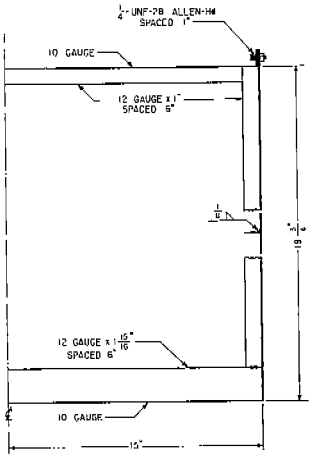

FIG. 3. MIDSHIP SECTION.

FIG. 4. EXPERIMENTAL MODEL.

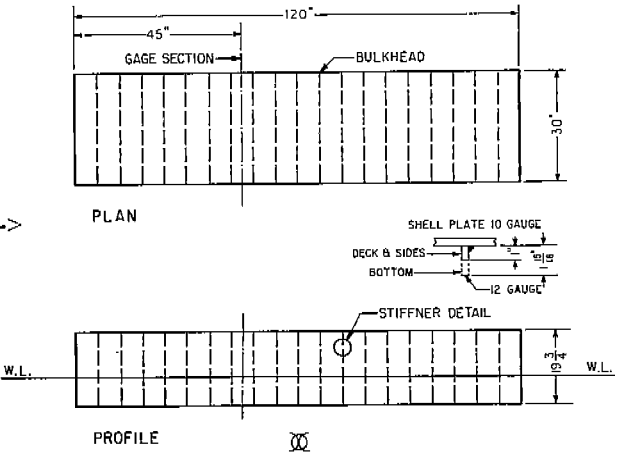

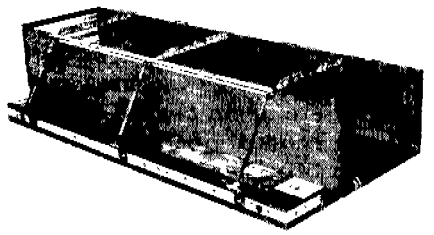

FIG. 5. MODEL BEFORE WELDING.

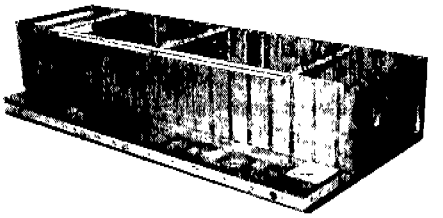

FIG. 6. MODEL AFTER WELDING.

geometrical similarity, these are not features whose presence will make important contributions to the experimental results desired. Their presence would, on the other hand, create difficult and expensive fabrication problems.

The midship section of the model is shown in Fig. 3. The model has a beam of 30 in. and a depth of 20 in. and a length of 10 ft, Fig. 4. The beam-depth ratio of 1.5 is somewhat below the current typical values of 1.8 to 2.1. This was done to permit a 20 inch depth, - the minimum considered usable from an access standpoint, - to be obtained from a single sheet of steel 6 ft in width. To minimize the amount of welding that had to be done, the bottom and both sides were formed from a single sheet of 10-gauge steel. The AISI C1015 hot-rolled sheet, which was pickled and oiled prior to fabrication, was carefully selected to be free of any mechanical defects. The only welding was that required for the attachment of the frames and the end flanges. The frames were fabricated from 12-gauge steel, and then welded to the hull and deck plating. The model is shown in Fig. 5 before the frames were welded in place. Figure 6

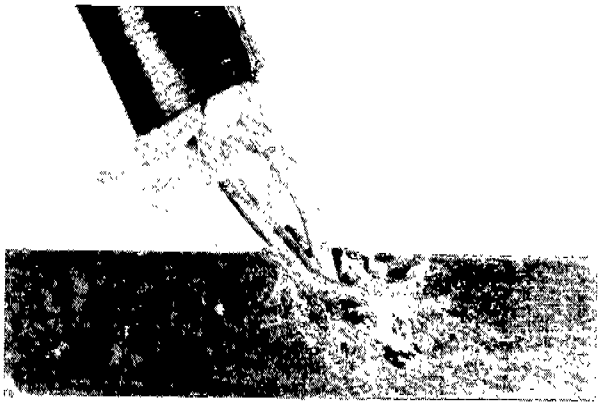

FIG. 7. CROSS SECTION OF THERMOCOUPLE INSTALLATION.

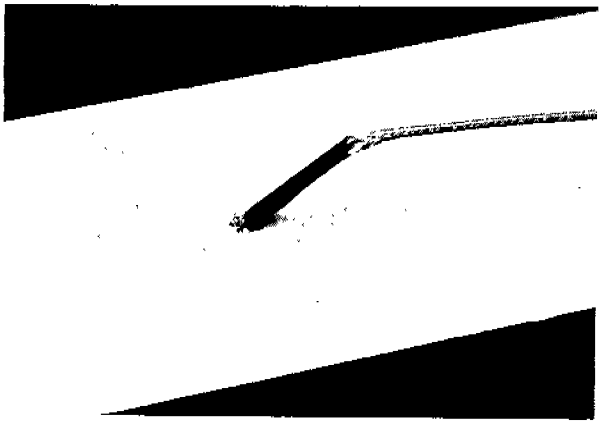

FIG. 8. SURFACE VIEW OF THERMOCOUPLE INSTALLATION.

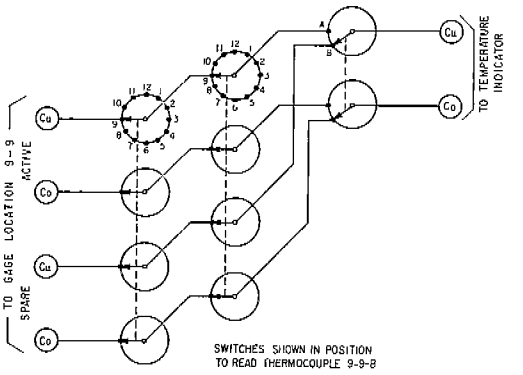

FIG. 9. SCHEMATIC DIAGRAM OF THERMOCOUPLE SWITCHING NETWORK.

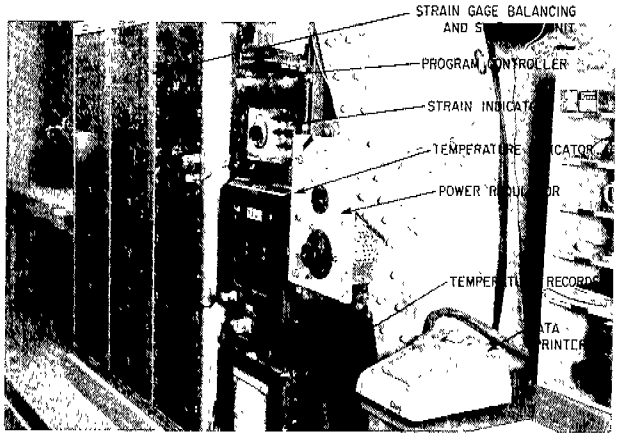

FIG. 10. INSTRUMENTATION CONTROL PANEL.

shows the model after the frames had been welded in place. Following completion of all welding, the model was stress relieved at 1150 F for one hour, and then sand blasted to a bright metal condition.

Instrumentation. To carry out the objectives of this study, it was necessary to make both temperature and strain measurements on the model. Since the temperature measurements were also involved in the measurement of strain, they will be discussed first.

Temperature Measurements

The temperatures at the various locations were measured by use of copper-constantan thermocouples with specially selected "hi-accuracy" thermocouple wire. The thermocouples themselves were made by twisting the two wires together, to form a junction, and then soldering the junction. As shown in Fig. 7, the holes into which the thermocouples were peened were drilled at an angle of 45° to the plane of the plating. This technique was used to permit accurate depth control, and also to simplify the peening operation. In every case the thermocouples were installed from the inside of the model. This was done to prevent difficulties which would be encountered if the thermocouples were located in the presence of water.

The thermocouple wires were led from the model to a switching network, and thence to the indicators and recorders. The temperature measuring instruments themselves consisted of a temperature indicator with digital readout, and a 16-channel temperature recorder. The digital output was connected directly to the linear slide wire on the temperature indicator. Since the copper-constantan thermal E.M.F. curve is a nonlinear function of temperature, the digital output is in a nonlinear form. The overall accuracy of the temperature measurements was within $\pm$ 1/2 F.

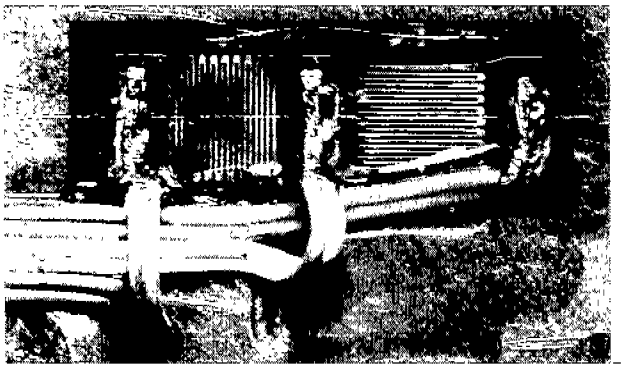

FIG. 11. TYPICAL STRAIN GAGE INSTALLATION.

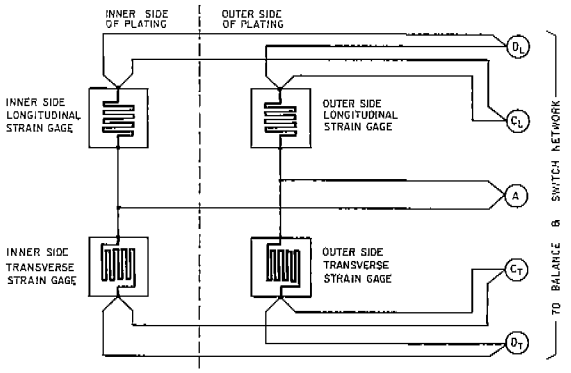

FIG. 12. SCHEMATIC DIAGRAM OF STRAIN GAGE WIRING.

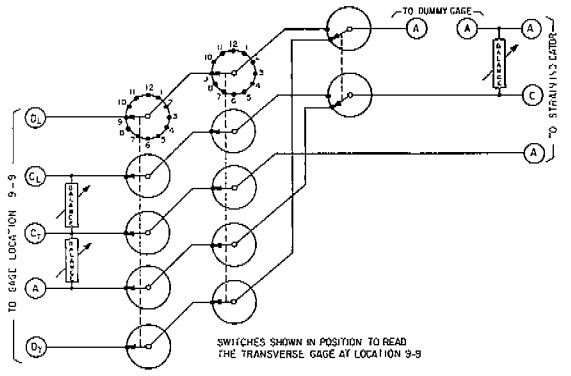

FIG. 13. SCHEMATIC DIAGRAM OF STRAIN GAGE SWITCHING AND BALANCING NETWORK.

A picture of a sample thermocouple installation is shown in Figs. 7, 8. The schematic wiring diagram for the thermocouple switching network is given in Fig. 9, and the temperature measuring instruments are shown in Fig. 10.

Strain Measurements

In the presence of temperature gradients, the accurate measurement of strain in small structures becomes quite difficult since electric strain gages are, in general, highly sensitive to temperature changes. Only by very careful design and installation can acceptable strain measurements be made in the presence of changing temperature. In large structures, where the typical dimensions of the structure are many orders of magnitude larger than the typical dimension of the strain gage, the thermal compensation of the strain gage may be carried out by use of "dummy" compensating gages. These gages are subjected to the same temperature environment as the "active" gages, but are not subjected to mechanical strain. By properly connecting these gages in the bridge circuit, it is possible to obtain thermal compensation with relative ease. This is the method used by Meriam[1] in the measurements on the SS Boulder Victory. However, in the case of small structures, the use of the "dummy" compensating gage is, in general, not feasible, since it is difficult to insure that the "dummy" compensating gage will be subjected to the same thermal environment as the active gage. When the use of the "dummy" compensating gages is not feasible, the alternative approach is to obtain the strain-gage characteristics as a function of temperature, and apply a suitable correction to the strain-gage readings. This, of course, implies that the temperature must be measured at each strain-gage location when the strain gage is read. Since the temperature distribution must be obtained anyway, this is not a serious obstacle. The calibration of the strain gages with respect to the temperature strain, or "apparent strain" as it is usually called, and the gage-factor calibration are discussed in Appendix C.

A closeup view of a typical gage installation is shown in Fig. 11. Inspection of this photograph clearly shows the construction of the foil gage and also the wiring connected thereto. Each half of the gage has three wires attached to it which compensates for the temperature sensitivity of the copper lead wire. This technique of compensation is known as the "three-wire" compensation circuit. It consists of arranging lead wire so that equal amounts of wire exposed to temperature variations appear in adjacent arms of the measuring bridge. Figures 12 and 13 together show

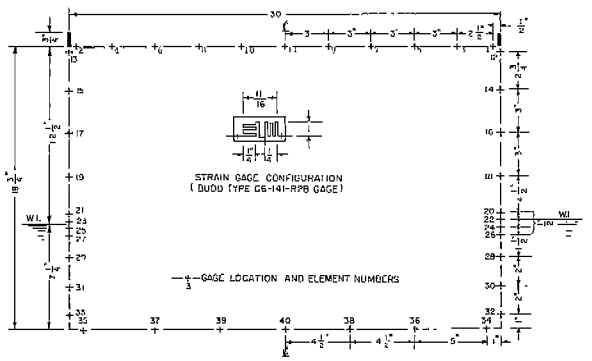

FIG. 14. GAGE LAYOUT, TRANSVERSE SECTION.

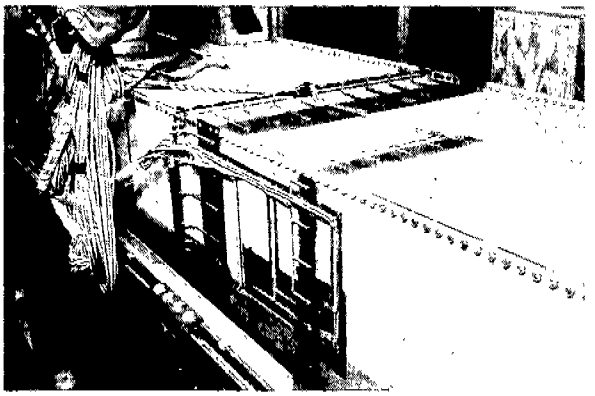

FIG. 15. VIEW OF TRANSVERSE TEST SECTION.

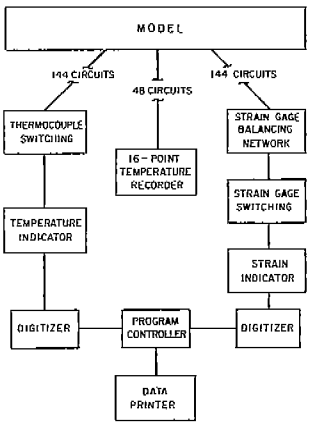

FIG. 16. BLOCK DIAGRAM OF INSTRUMENTATION.

the schematic wiring diagram for the strain gages.

To compute the longitudinal stress in the model, it is clear from Eq. 5 that both longitudinal and transverse strains must be measured. Further, it is absolutely necessary to make the strain measurements so that the effect of local plate bending is eliminated from the strain measurements. By making measurements on both sides of the plate, the effects of local bending can be eliminated either by computation or directly by the electrical circuitry. On this model, the cancellation was carried out by electrical means.

A common "dummy" gage in the bridge circuit was maintained at a constant temperature by means of a controlled bath. The switching network which was used was converted from existing equipment used in a prior investigation.[1] In addition, a balance network was designed and installed to permit rapid and easy balancing of all strain-gage circuits. The strain readings were made with an automatic servo-balanced Wheatsone bridge. This instrument was also provided with a digital read-out device.

The location of the strain gages on the main transverse test section is shown in Fig. 14, and a photograph of the test section may be seen in Fig. 15.

Data Acquisition

Both the temperature and the strain readings were recorded in digital form by use of a semi-automatic recorder. The data were printed on a paper tape on command of the operator of the switching panel. The data printer may be seen in Fig. 10. A block diagram of the entire instrumentation system is shown in Fig. 16.

Experimental Procedure. To obtain a set of experimental data from the model for given thermal loading conditions, the following steps were executed:

a. After the model and water had reached thermal equilibrium, all strain-gage circuits were balanced, and initial readings of strain and temperature were taken.

b. The heating system was activated and a steady-state temperature distribution was produced.

c. A final set of temperature and strain readings were then taken.

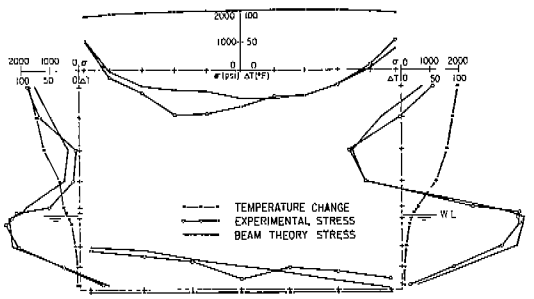

FIG. 17. LONGITUDINAL STRESS ACROSS TRANSVERSE MIDSHIP SECTION SYMMETRICAL TEMPERATURE DISTRIBUTION.

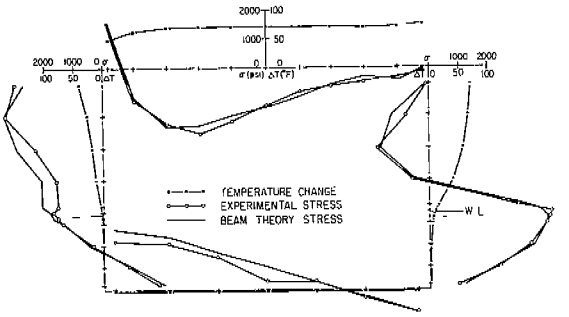

FIG. 18. LONGITUDINAL STRESS ACROSS TRANSVERSE MIDSHIP SECTION ASYMMETRICAL TEMPERATURE DISTRIBUTION.

This entire sequence took from three to five hours depending on room temperature, available steam supply, and the desired temperature distribution.

Data Reduction. The first step in the data reduction was to process the digital data on the output tape. The temperature readings were converted to actual temperatures via the calibration curve shown in Appendix C. Next the strain readings were corrected according to

$$e = e_R - e_A \tag{8}$$

where e = actual strain

e_R = strain reading

e_A = apparent strain

The apparent strain was determined from the apparent strain curve for the gage in question and the temperature just obtained. This procedure was carried out for initial readings at ambient temperature and also for the final readings taken at some elevated temperature. The difference between final and initial corrected readings yields the temperature change and the change in strain caused by the induced stress. The changes in strain are substituted into the appropriate stress strain law, Eq. 5.

$$\sigma_x = \frac{E}{1-\nu^2}[e_x + \nu e_y]$$

$$\sigma_y = \frac{E}{1-\nu^2}[e_y + \nu e_x] \tag{5}$$

to obtain the longitudinal and transverse thermal stresses respectively.

Next the resultant forces and moments acting on the section caused by the induced stresses were computed as an overall check on the experimental results. Ideally, the resultant force and moment should, of course, be zero. Practically, they should be negligible, compared with the absolute sum of forces and moments acting on the section.

The actual data reduction calculations were carried out on the IBM 704 digital computer at the University of California Computer Center. The computer program was coded by P. T. Lyman with the aid of the IBM 704 Fortran Programming System.[3] To carry out the data reduction described above for one test required two man-days of calculation and plotting when done by hand methods. When the computer is employed to do the required calculations, less than three man-hours are required to reduce one set of data. This includes all key-punching and plotting of results. The computer did its share of the work in just under one minute per test run.

Results. Two sets of experimental results are reported here to show the comparison between the stresses as calculated by the strength-of-materials method (described later) and as determined from the experimental model. One set of data is typical of a symmetrical temperature distribution, Fig. 17, and the second set is typical of an asymmetrical temperature distribution, Fig. 18. The complete set of experimental data, the calibration data, the section properties, and tabular results for these two tests are given in Appendix B.

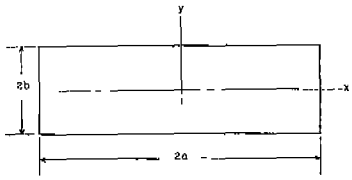

FIG. 19. COORDINATES FOR TWO-DIMENSIONAL PROBLEMS.

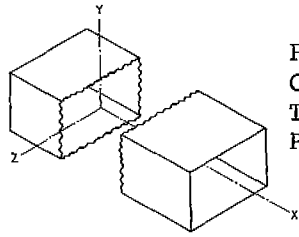

FIG. 20. COORDINATES FOR THREE-DIMENSIONAL PROBLEMS.

Tests were conducted to produce and measure the effects of longitudinal temperature gradients and transverse restraint on the model. The results were not conclusive and are not included for the reasons presented under the section on Discussion, Conclusions, and Recommendations.

THEORETICAL

General. One of the major purposes of the project was to investigate and develop, if possible, a theoretical solution to the thermal stresses in a hull girder, which could be used or adapted for use in a design office. Further it was desired to demonstrate the conditions under which the rather simple beam-theory or strength-of-materials solution provided an adequate prediction for design purposes.

Strength-of-Materials Solution. The longitudinal thermal stresses in a freely-supported elastic beam of infinite length subjected to an arbitrary transverse temperature distribution invariant with the length has been shown to be given by (9)

$$\sigma_x = -E\alpha T + \frac{1}{A}\int E\alpha T\,dA + \frac{y}{I_z}\int yE\alpha T\,dA + \frac{z}{I_y}\int zE\alpha T\,dA \qquad (9)$$

when applied to the beam with x as the longitudinal axis, y as the vertical axis, and z as the horizontal transverse axis. Figures 19 and 20 show the coordinates used to describe both a two-dimensional beam (of finite length) and the three-dimensional beam of infinite length. Practically the beam does not need to be very long before the end effect for a finite-length beam becomes negligible at sections removed from the ends. For arbitrary temperature distributions not easily expressable as a simple function of the transverse coordinates, Eq. (9) may be rewritten in finite difference form as

$$\sigma_x = -E\alpha T + \frac{\Sigma E\alpha T\,\Delta A}{\Sigma \Delta A} + y\frac{\Sigma yE\alpha T\,\Delta A}{\Sigma y^2\,\Delta A} + z\frac{\Sigma zE\alpha T\,\Delta A}{\Sigma z^2\,\Delta A} \qquad (10)$$

which is the form used by Jasper[2] and in the SS Boulder Victory tests.[1] As mentioned in the previous section on experimental results, the stresses calculated from Eq. (10) for the measured temperature distributions of Figs. 17 and 18 are shown by the full line in each of these figures. Except for one small region in the deck to the left of the center line, Fig. 17, the agreement between beam theory and experiment is quite good.

Theory-of-Elasticity Solution to Two-Dimensional Problem. As a first step toward the development of a more complete solution to the three-dimensional problem, several two-dimensional problems were investigated to examine the end effect for a thermally loaded plate of finite dimensions and to develop a solution technique which would be applicable to the three-dimensional problem. Accordingly the configuration of Fig. 19 was used for these purposes.

It is well known that the field equation governing the solution of a two-dimensional thermo-elastic problem is

$$\nabla^4\varphi = -E\alpha\nabla^2 T \qquad (11)$$

where $\nabla^4 = \nabla^2\nabla^2$, $\nabla^2 = \frac{\partial^2}{\partial x^2} + \frac{\partial^2}{\partial y^2}$,

and φ is the airy stress function related to the stresses by

$$\left.\begin{aligned}\sigma_x &= \frac{\partial^2\varphi}{\partial y^2}\\ \sigma_y &= \frac{\partial^2\varphi}{\partial x^2}\\ \tau_{xy} &= -\frac{\partial^2\varphi}{\partial x\partial y}\end{aligned}\right\} \qquad (12)$$

If t and n represent coordinates tangent to and normal to a boundary, then the boundary

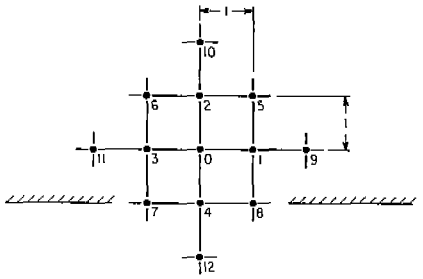

FIG. 21. NODE NUMBERING SYSTEM FOR SQUARE MESH.

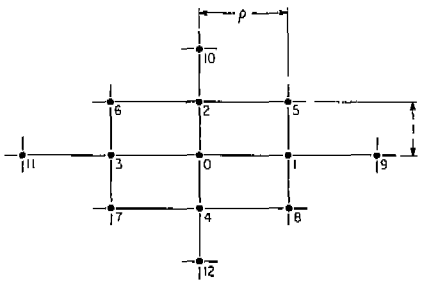

FIG. 22. NODE NUMBERING SYSTEM FOR RECTANGULAR MESH.

will be free of normal stress provided that $\varphi = a + kt$ along the boundary ($\sigma_n = \frac{\partial \varphi}{\partial t^2} = 0$) where a and k are constants. The boundary will be free of shear stress provided that $\frac{\partial \varphi}{\partial n} = 0$ since the shear would be given by $-\frac{\partial^2 \varphi}{\partial n \partial t}$. No loss of generality in the solution results by taking a = k = 0, so that the boundary conditions for the rectangular plate of Fig. 19 free of boundary stress are

$$\left.\begin{aligned} x = \pm a,\ \varphi = 0,\ \frac{\partial \varphi}{\partial x} = 0 \\ y = \pm b,\ \varphi = 0,\ \frac{\partial \varphi}{\partial y} = 0 \end{aligned}\right\} \qquad (13)$$

A number of mathematical approaches to the solution of Eq. (13) with the above boundary conditions were investigated.[5] Except for the simplest form of temperature distribution no method was found which provided an approach without excessive and cumbersome calculations, generally unsuitable for adaptation to design procedures. Consequently, attention was directed toward a digital computer solution of Eq. (11) written in finite difference form. The IBM 704 and later the 7090 large scale digital computers were available to the project and were used for this purpose.

The finite difference equivalents of Eqs. (11) through (13) for the case of a square finite difference mesh may be obtained from "Bickley's Formulas", found in almost any reference on numerical analysis. Figure 21 shows the relative node numbering system for all of the following finite difference equations. The finite difference equivalent to Eq. (11) is

$$20\varphi_0 - 8\Sigma\varphi_1 + 2\Sigma\varphi_5 + \Sigma\varphi_9 + E\alpha[\Sigma T_1 - 4T_0] \qquad (14)$$

where $\Sigma\varphi_1 = \varphi_1 + \varphi_2 + \varphi_3 + \varphi_4$

$\Sigma\varphi_5 = \varphi_5 + \varphi_6 + \varphi_7 + \varphi_8$

$\Sigma\varphi_9 = \varphi_9 + \varphi_{10} + \varphi_{11} + \varphi_{12}$

The stresses are determined from the following set of difference relations

$$\sigma_x = \frac{\partial^2 \varphi}{\partial y^2} \approx \varphi_2 + \varphi_4 - 2\varphi_0 \qquad (15a)$$

$$\sigma_y = \frac{\partial^2 \varphi}{\partial x^2} \approx \varphi_1 + \varphi_3 - 2\varphi_0 \qquad (15b)$$

$$\tau_{xy} = -\frac{\partial^2 \varphi}{\partial x\, \partial y} \approx (\varphi_6 + \varphi_8 - \varphi_5 - \varphi_7)/4 \qquad (15c)$$

In the foregoing equations the mesh size has been normalized to one, so that no explicit reference to the mesh size appears.

From a standpoint of computational efficiency, it is desirable to have the equivalent of the above equations for a rectangular finite difference mesh. The derivation of the finite difference equations for the rectangular mesh shown in Fig. 22 may be carried out using either the interpolating parabola technique, or the Taylor series expansion technique. Both of these methods are well documented in the literature.[6-9] The finite difference expression for Eq. (11) using a rectangular mesh with length to height ratio of ρ is given by

$$6(1+\rho^4)\varphi_0 + 8\rho^2\varphi_0 - 4(\varphi_1+\varphi_3) -$$

$$4\rho^4(\varphi_2+\varphi_4) + (\varphi_9+\varphi_{11}) + \rho^4(\varphi_{10}+\varphi_{12}) +$$

$$2\rho^2\Sigma\varphi_5 - 4\rho^2\Sigma\varphi_1 + \rho^2 E\alpha[(T_1+T_3) +$$

$$\rho^2(T_2+T_4) - 2(1+\rho^2)T_0] = 0 \qquad (16)$$

The stresses are determined with the aid of the following corresponding equations.

$$\sigma_x = \frac{\partial^2\varphi}{\partial y^2} \approx (\varphi_2+\varphi_4-2\varphi_0) \qquad (17a)$$

$$\sigma_y = \frac{\partial^2\varphi}{\partial x^2} \approx (\varphi_1+\varphi_3-2\varphi_0)/\rho^2 \qquad (17b)$$

$$\tau_{xy} = -\frac{\partial^2\varphi}{\partial x\partial y} \approx (\varphi_6+\varphi_8-\varphi_5-\varphi_7)/4\rho \qquad (17c)$$

The appropriate field equations must be solved, subject to the proper boundary conditions, which for the case of a freely supported beam are given by Eqs. (13). Inspection of Fig. 21 indicates that when the finite difference equation for a node adjacent to a boundary is being written, there is apparently an unknown value of the stress function outside the physical boundary. This unknown value lying outside the boundary is commonly called an image point, and may be determined from the remaining boundary condition. To insure a zero normal derivative at the boundary, the image point must take on the same value as the node point for which the equation is being written. Hence, the image point may be eliminated explicitly from the nodal equation.

To demonstrate the effect of the mesh size on the convergence of the finite difference solution, a plate with a side ratio of two, as shown in Fig. 23 was used. The plate was subjected to the piecewise linear temperature distribution, shown in Fig. 23, which has no variation in the x-direction. For this problem, a square finite difference mesh was employed, and hence, Eq. (14) is the appropriate difference equation. Three mesh sizes were considered--"mesh 1" required the solution of 21 equations, "mesh 2" required the solution of 105 equations, and "mesh 3" required in general the solution of 465 equations. In this particular case, there is a line of symmetry and a line of asymmetry, so that the number of independent equations are 8, 32, and 112 respectively. (It should be pointed out that from a computational standpoint, it is very important to take advantage of symmetry or asymmetry whenever it exists, since, at best, the work required to solve a system of equations is proportional to the cube of the number of unknowns.) A tabular comparison of the solutions for the longitudinal stresses (x-stresses) is shown in Table 1. As a further comparison, the results of an Aiken type extrapolation[9-10] are also shown in the table, and the errors shown are in reference to these extrapolated values. Figures 24, 25, and 26 show the plotted results of this comparison for "mesh 2" and "mesh 3." "Mesh 1" is not shown since it differs from a satisfactory solution by too large a margin.

To determine the extent of the "end effect" in the beam, a similar problem was solved in which the length of the beam was varied. Figure 27 shows the beam and the temperature distribution used. The length of the beam, $2\rho a$, was taken as 2a, 4a, and 6a, where a is the depth of the beam. The change of length was made by changing from a square finite difference mesh ($\rho = 1$) to a rectangular mesh of $\rho = 2$ and $\rho = 3$. The appropriate difference equation is (16).

The mesh size used corresponds to "mesh 2" of the previous example. The results of these calculations are shown in Figs. 28, 29, and 30. In Fig. 30 the apparent effect of change of length on the shear stresses at the end of the beam is not a real effect. It appears from the plot that the stresses tend to decrease with increasing length; however, this apparent effect is due to the fact that the peak stresses actually occur between the last two mesh points in the longer beams thus preventing a determination of the peak values. The curves shown are plotted with peak calculated values. It would be possible to show this by adjusting the mesh size at the ends of the beam. However, there does not seem to be any justification for doing so in terms of the object of this study.

One additional two-dimensional thermal stress solution was studied, and that is a comparison of the finite difference solution with the solution due to Heldenfels and Roberts.[11] The problem is defined by Fig. 31. The finite difference solution required the solution of only 54 equations, since use was made of the existing symmetry and asymmetry. The comparisons of the two solutions are shown

TABLE I. EFFECT OF MESH SIZE ON CONVERGENCE OF SOLUTION.

ROW	COL	MESH 1 STRESS PSI	MESH 2 STRESS PSI	MESH 3 STRESS PSI	EXTRAPOLATED STRESS PSI	MESH 1 ERROR PCT	MESH 2 ERROR PCT	MESH 3 ERROR PCT
1	1	0	0	0	0	0.0	0.0	0.00
1	5	2540	3575	3701	3718	31.7	3.9	0.46
1	9	2575	3636	3721	3728	30.9	2.5	0.19
1	13	2572	3636	3721	3728	31.0	2.5	0.19
1	17	2571	3636	3721	3728	31.0	2.5	0.19
1	17				(3750)*			
5	1	0	0	0	0	0.0	0.0	0.00
5	5	-2540	-3129	-3117	-3117	18.5	-0.4	0.00
5	9	-2575	-3182	-3140	-3148	18.2	-1.1	0.25
5	13	-2572	-3182	-3140	-3148	18.3	-1.1	0.25
5	17	-2571	-3182	-3140	-3148	18.3	-1.1	0.25
5	17				(-3125)*			
9	1	0	0	0	0	0.0	0.0	0.00
9	5	0	0	0	0	0.0	0.0	0.00
9	9	0	0	0	0	0.0	0.0	0.00
9	13	0	0	0	0	0.0	0.0	0.00
9	17	0	0	0	0	0.0	0.0	0.00
9	17				(0)*			

* BEAM THEORY PREDICTION

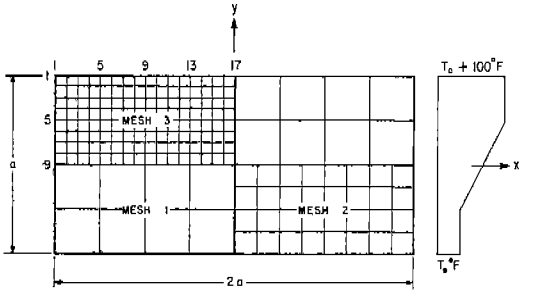

FIG. 23. MESHES USED TO DEMONSTRATE THE EFFECT OF MESH SIZE ON CONVERGENCE OF THE SOLUTION.

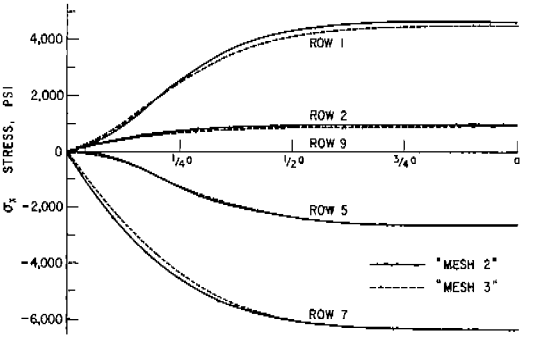

FIG. 24. EFFECT OF MESH SIZE ON THE CALCULATED STRESSES HORIZONTAL NORMAL STRESS.

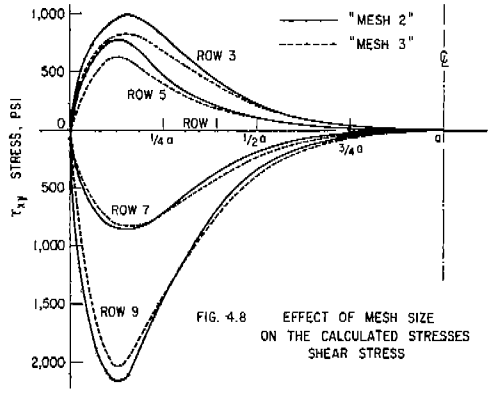

FIG. 25. EFFECT OF MESH SIZE ON THE CALCULATED STRESSES SHEAR STRESS.

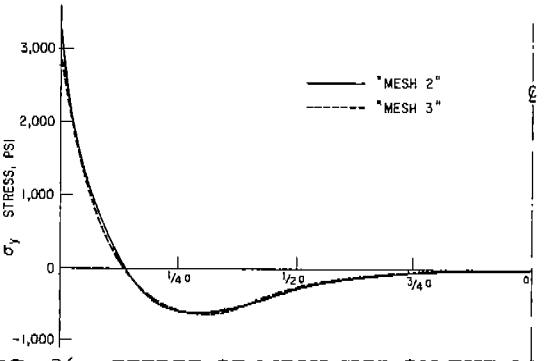

FIG. 26. EFFECT OF MESH SIZE ON THE CALCULATED STRESSES VERTICAL NORMAL STRESS. ROW 5.

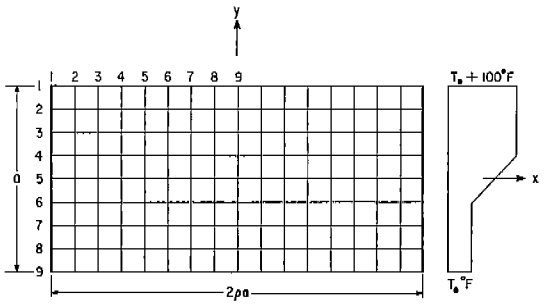

FIG. 27. MESH USED TO DEMONSTRATE THE "END EFFECT" FOR PLATES OF DIFFERENT LENGTHS.

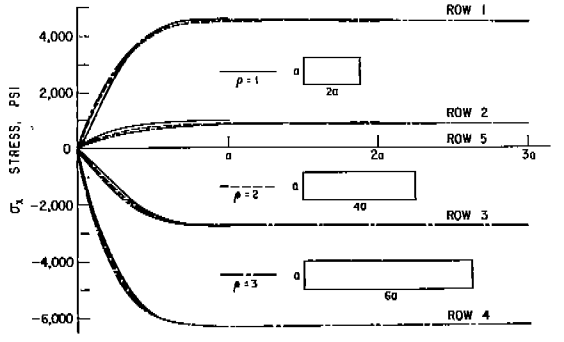

FIG. 28. COMPARISON OF END EFFECTS FOR PLATES OF DIFFERENT LENGTHS HORIZONTAL NORMAL STRESS.

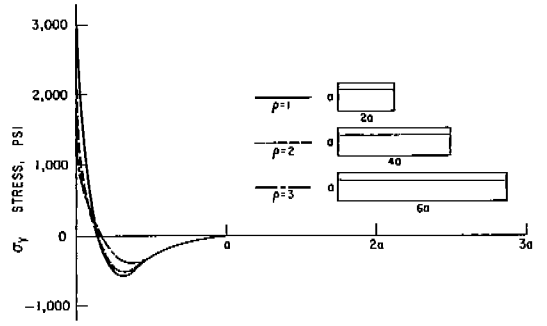

FIG. 29. COMPARISON OF END EFFECTS FOR PLATES OF DIFFERENT LENGTHS VERTICAL NORMAL STRESS. ROW 3.

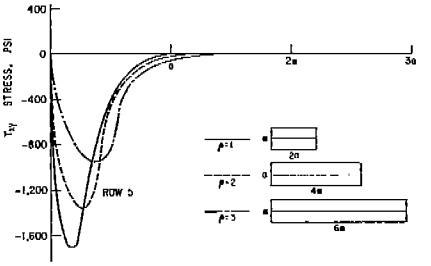

FIG. 30. COMPARISON OF END EFFECTS FOR PLATES OF DIFFERENT LENGTHS SHEAR STRESS. ROW 5.

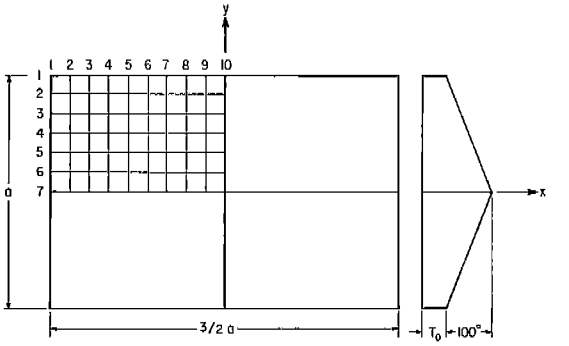

FIG. 31. MESH USED FOR FINITE DIFFERENCE SOLUTION.

in Figs. 32 through 35.*

The foregoing analyses and comparisons of the finite-difference computational approach to the flat-plate thermal stress problem were made and presented to help establish the validity of the method used, before extending the method to the three-dimensional folded-plate model simulating a ship. The following general conclusions may be drawn from the preceding studies:

1. The study of the effect of mesh size clearly indicates the relative mesh size required for design accuracy. "Mesh 2" agreed to within about three percent of the final extrapolated answer in all cases.

2. For plates with a side ratio of two or greater, the longitudinal normal stress at the center section of the plate agreed to within one percent of the infinite beam solution. This conclusion agrees with the conclusions of Horvay.[12]

3. The end effect in the plate is confined to a square region at each end on the plate irrespective of the length of the plate. This conclusion, together with the previous one, indicates that the strength-of-materials solution may be used with confidence, in the region where there is absence of longitudinal temperature gradients and/or transverse restraints.

* This problem was set up and solved with the aid of the IBM 7090 in approximately four hours (actual computing time was about 50 seconds.)

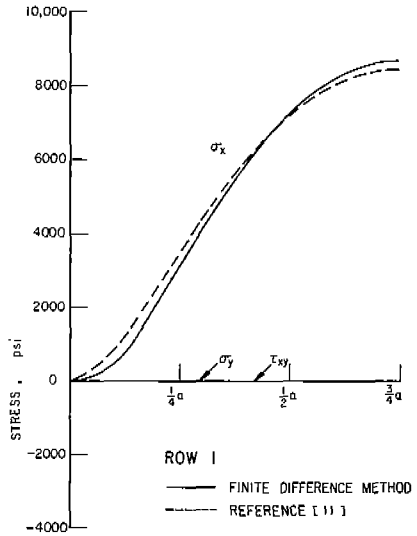

FIG. 32.

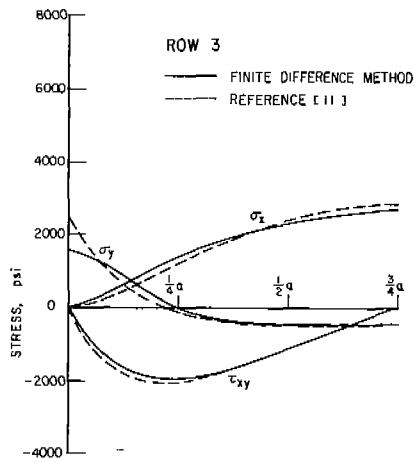

FIG. 33.

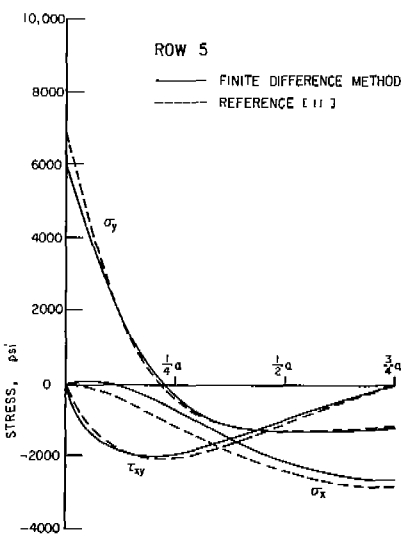

FIG. 34.

FIGS. 32--35. COMPARISON OF FINITE DIFFERENCE SOLUTION WITH THAT OF HELDENFELS AND ROBERTS.[11]

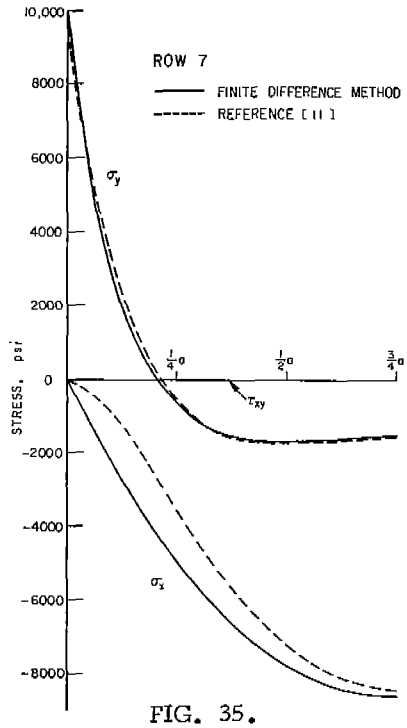

FIG. 35.

4. The most important result arising from the solutions presented is the demonstration of the ease and speed with which a complete stress distribution may be obtained for quite arbitrary temperature distributions.

Theory-of-Elasticity Solution to Three-Dimensional Problem. To effect a three-dimensional solution for the simulated ship structure, using the same technique as in the two-dimensional strip, consider the box beam shown in Fig. 36. This beam consists of four plane-stress elements joined by appropriate boundary conditions. In using this beam for analysis of thermal stresses in ships, an implicit assumption is that local bending effects, due to general temperature distributions, are small. In other words, it is assumed that the girth stresses at the corners of the beam are negligibly small. The local bending which can arise from temperature gradients through the plating and stiffeners may be treated with existing techniques, and incorporated into a general solution by means of the superposition principle. A further assumption which needs examination is the use of a prismatic beam to represent a ship for the purpose of thermal stress analysis. It is clear that the majority of all ships have a hull form which may be approximated for a considerable

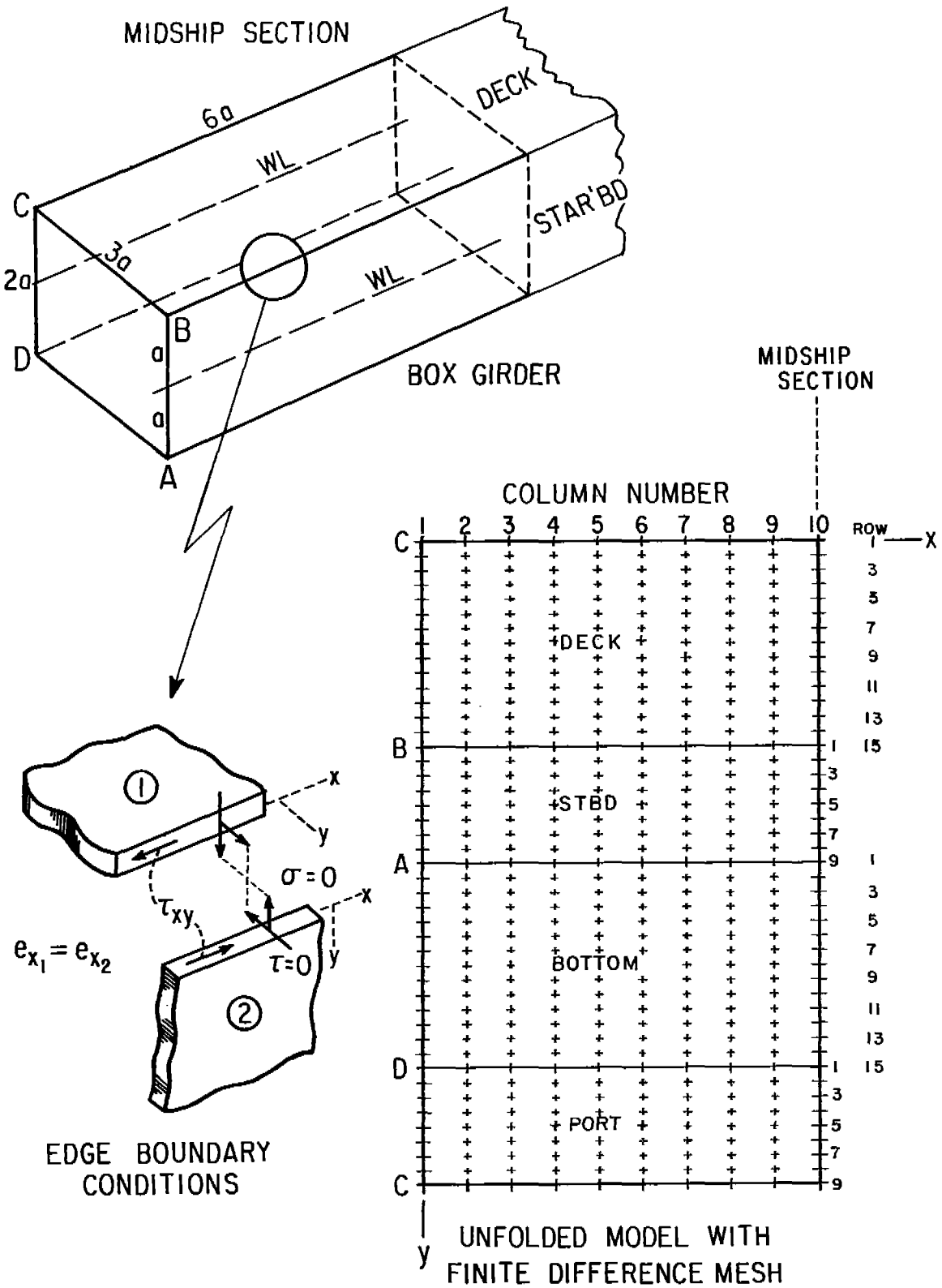

FIG. 36. THREE DIMENSIONAL MATHEMATICAL MODEL FOR COMPUTER SOLUTIONS.

length by a prismatic section. Hence, if it can be shown that the end effects in the beam are small, the prismatic beam solution for the ship will yield valid results in the region of maximum interest, i.e., the midship half-length.

The boundary conditions which must be satisfied at the corners of the beam are shown in Fig. 36. From equilibrium considerations, it is clear that the in-plane shear stresses on any adjacent elements must be equal in magnitude. From the assumption that the local bending effects are negligible, it follows that the girth stress (y-stress) vanishes on the boundaries. To assure compatibility of the elements, it is necessary that the longitudinal displacements (x-displacements) be equal along the common boundaries. The boundary conditions on the ends of the beam are that the longitudinal stresses and the in-plane shear stresses vanish.

The boundary conditions along two typical elements labeled (1) and (2) may be written as

$$(\tau_{xy})_1 = (\tau_{xy})_2 \tag{18}$$

$$(\sigma_y)_1 = (\sigma_y)_2 = 0 \tag{19}$$

$$(u)_1 = (u)_2 \tag{20}$$

It follows directly from the strain-displacement equation

$$e_x = \frac{\partial u}{\partial x} \tag{21}$$

that compatibility condition (Eq. 20) is equivalent to

$$(e_x)_1 = (e_x)_2 \tag{22}$$

Further, it follows from the stress-strain equation

$$e_x = \frac{\sigma_x}{E} - \nu \frac{\sigma_y}{E} \tag{23}$$

and Eq. (19) that the compatibility equation is also equivalent to

$$(\sigma_x)_1 = (\sigma_x)_2 \tag{24}$$

It has been shown now, that all three stress components (σ_x, σ_y, τ_{xy}) are continuous functions at the boundaries of any two adjacent elements. Since the three components of stress are derivable from the Airy stress function, Eq. (12) via the three-second partial derivations, it follows that the Airy stress function and its first two partial derivations are continuous functions across the common boundaries.

An integration of Eq. (19) in terms of the Airy function

$$\int\int \sigma_y \, dx \, dx = \int\int \frac{\partial^2 \varphi}{\partial x^2} dx \, dx = 0$$

along the common boundary yields

$$\varphi = x\, f(y)]_{y=0} + g(y)]_{y=0} \tag{25}$$

or

$$\varphi = xC_1 + C_2 \tag{26}$$

It is thus seen that the most general form for the stress function along a common boundary is a linear function in the longitudinal coordinate. The two arbitrary constants may be determined from the values of the stress function on the free ends of the beam. Since the addition of a general linear function to the stress function will have no effect on the derived stresses, it is useful from a computational standpoint to take the stress function on the free boundaries at the ends of the beam as zero, and hence, also along the common boundaries.

To summarize, the boundary conditions which must be satisfied in solving for the stress function for the box girder are:

1. The stress function is taken as zero on all free and common boundaries.

2. The normal derivatives of the stress function on the free boundaries shall be zero.

3. The stress function and its first two derivatives shall be continuous across the common boundaries.

As in the two-dimensional case, the field equation is Eq. (11). In fact, from a mathematical point of view, the solution of the beam by the above technique has been reduced to a two-dimensional plane stress problem, even though the beam itself is a three-dimensional structure.

For solutions of the three-dimensional box girder, the mathematical model shown in Fig.

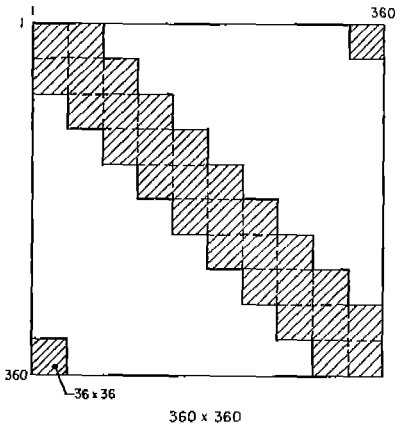

FIG. 37. SCHEMATIC REPRESENTATION OF THE "BAND MATRIX" REPRESENTING THE BOX BEAM SOLUTION.

36 was used. This model, which represents just one-half of the total girder, is suitable for any temperature distribution which is symmetric about the midship section. (This restriction is one of convenience, not necessity). This model is represented by 440 mesh points, 80 of which represent boundary points; hence, there are only 360 unknown values of the stress function to be determined. The mesh size used is the same as shown in Fig. 28 with $\rho = 3$. For the two-dimensional problems studied, this mesh size yielded results which were within about three percent of extrapolated values.

To determine the stresses in the model due to a particular temperature distribution, it was necessary to solve the 360 finite difference equations for each desired temperature distribution. In principle, all that is necessary is to find the inverse of the coefficient matrix for the equation. However, the determination of the inverse of a general matrix of this size is a rather time-consuming task, even on modern digital computers. In solving the two-dimensional problems, most of which involved about 105 equations, the time on the IBM 704 for inversion was about ten minutes. Since the work to invert a system of equations is at best proportional to the cube of the number of equations, the direct inversion of 360 equations by the same technique would involve about six and one-half hours of IBM 704 time. Fortunately, the coefficient matrix for the model has certain properties which permit a substantial saving in computational time. Figure 37 shows a schematic representation of the finite difference equations used for the chosen model. The small shaded squares represent nonnull sub-matrices. The unshaded areas represent null sub-matrices. It should be noted that although there are some very fast routines for solving equations which have a structure similar to that shown in Fig. 37, the two nonnull elements in the corners of the diagonal render them useless. The technique used to solve these equations was to replace the given set of 360 equations by ten equations whose coefficients are the 36 x 36 submatrices. These ten equations are then solved by a Crout-type elimination procedure.[13] This method makes full use of the null submatrices and requires only the inversion of ten 36 x 36 matrices. On the IBM 704 this method required 18 minutes for the reduction up to the point where the first temperature distribution was required. An additional 3.6 minutes was required to complete the reduction and to compute the stresses for each desired temperature distribution. The computer program yielded not only the three coordinate stresses, but also the principal stresses and directions. The IBM 704 time to obtain the complete solutions for m different temperature distributions for the described model was

$$T = 18 + 3.6 \text{ minutes}$$

The reduction-inversion method used for this model is almost 2300 percent faster than the direct inversion of a general matrix of this size.

The model described previously in Fig. 36 was used to study a wide range of temperature distributions. Included in a systematic variation were the effects of four different transverse temperature distributions superimposed on five different waterlines and two different longitudinal temperature distributions. One complete set of results for one of the cases studied is presented in Appendix A as an example of the results which may be obtained from this type of analysis. This case represents a half-depth waterline, a symmetrical transverse temperature distribution with no longitudinal temperature variation. The tabular data presented for this case are direct copies of the output pages from the IBM 704. A graphical representation of these results is given in Figs. 38 through 43. Figure 38 shows the longitudinal stress plotted at various transverse stations along the length of the model. Also plotted at the midship section is

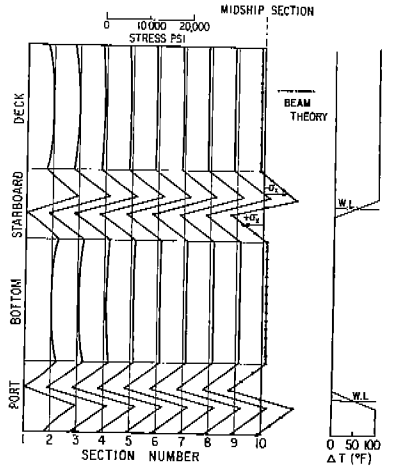

FIG. 38. LONGITUDINAL STRESSES.

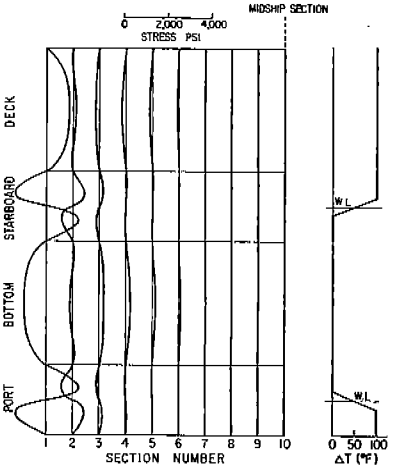

FIG. 39. TRANSVERSE STRESSES.

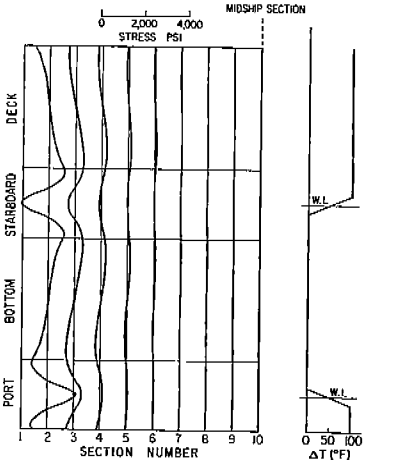

FIG. 40. COORDINATE SHEAR STRESSES.

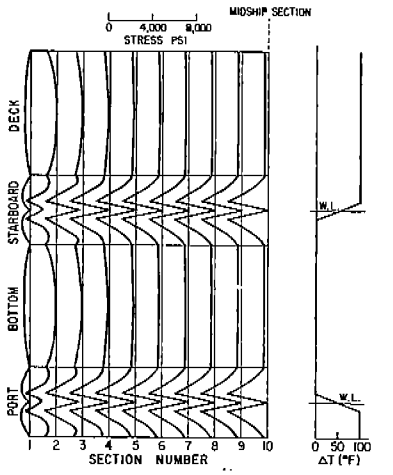

FIG. 41. MAXIMUM SHEAR STRESSES.

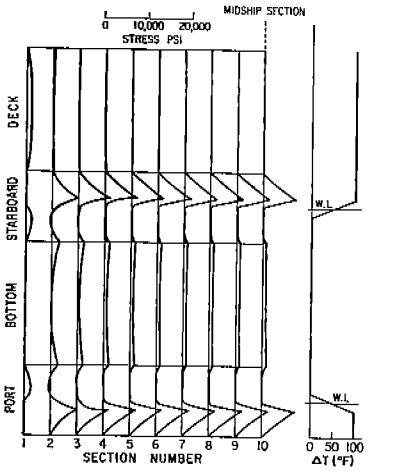

FIG. 42. MINIMUM PRINCIPAL STRESSES.

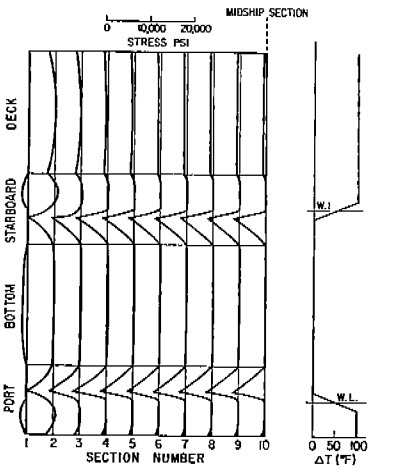

FIG. 43. MAXIMUM PRINCIPAL STRESSES.

FIGS. COMPUTER SOLUTION OF STRESSES FOR SYMMETRICAL TEMPERATURE DISTRIBUTION.

the strength-of-materials solution for a beam with the same cross section but of infinite length. These two solutions agree almost exactly over the entire cross section, the difference at the point of maximum longitudinal stress being about 0.20 percent.

Two striking features of these data are seen on further inspection of the six figures. First is the comparison of the amount of information supplied by the elastic solution as contrasted with the strength-of-materials solution. The second feature, noted previously in the two-dimensional problem, is that the end effect is very localized. This fact is best seen by inspection of the plot of transverse stresses and the plot of coordinate shear stresses, Figs. 39 and 40. Figures 41, 42, and 43 show the distribution of the magnitudes of maximum shear and minimum and maximum principal normal stresses, respectively.

An example of the studies made on the effect of change of waterline, with no longitudinal variation in temperature, Fig. 44, shows the midship longitudinal stress distribution. As in the previous case presented, the strength-of-materials solution differs from the elastic solution by less than one percent.

Figure 45 is a plot of the longitudinal stresses plotted at various transverse sections of the beam, for an asymmetrical transverse temperature distribution with no longitudinal temperature variation. The most important feature of this plot is that the strength-of-materials solution does not agree with the elastic solution as well as in the previous cases, even though the agreement in regions of peak stress seems to be good. In fact the results of all cases of asymmetrical temperature distribution show this disagreement, while all cases of symmetrical transverse temperature distribution show a striking agreement.

To demonstrate that the disagreement of the longitudinal stresses in the case of asymmetrical transverse temperature distributions is a real effect and not a defect in the solution of the problem, a special case was solved. This case consisted of an asymmetrical transverse temperature distribution which when reflected upon itself and superimposed, yielded a symmetrical transverse temperature distribution. The reflection and superposition of the asymmetrical case yielded the results of the symmetrical case exactly, and hence the departure from the strength-of-materials solution must be correct.

Figure 46 shows the effect of waterline depth on the longitudinal stresses at the midship section for an asymmetrical temperature distribution. Figure 47 is a plot of the stress trajectories for the asymmetrical temperature distribution used in Figs. 45 and 46.

Figure 48 shows a limited amount of information on the effect of longitudinal temperature variations. With the exception of the longitudinal variation in temperature between sections 6 and 7, the temperature distribution from sections 7 to 10 is the same as shown in Figs. 38 through 43. Curves B and C represent the behavior of the stresses along longitudinal sections of maximum stress corresponding to the case of no longitudinal temperature variation. The stresses along section B rise slightly as the temperature gradient is reached and then rapidly vanish as the temperature gradient vanishes. The stresses along section C behave in a similar manner except that they never show the slight rise before the abrupt drop is reached in the region of the temperature gradient. On the other hand, the longitudinal stresses along section A, which are normally in a region of low stresses, show abrupt peaks at the beginning and end of the longitudinal temperature gradient.

EFFECT OF TRANSVERSE RESTRAINT

The elastic-beam model previously considered does not account for the presence of discrete transverse stiffening which is caused by transverse bulkheads and deep web frames. An insight into the nature of the effects of this restraint may be had by examining the case of complete transverse restraint. It is true, of course, that total transverse restraint can never be achieved in any real structure, but the case of total transverse restraint represents an upper bound to the problem.

Consider a two-dimensional beam with the x-axis as the longitudinal axis and the y-axis as the transverse axis. Along one end of the beam at x = const. let

$$u = 0$$
$$v = 0 \qquad (27)$$

where u = the longitudinal displacement
v = the transverse displacement

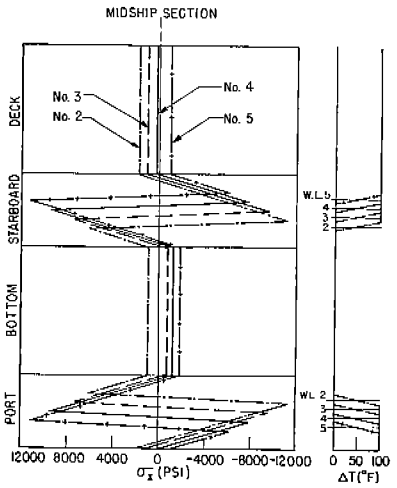

FIG. 44. EFFECT OF DRAFT ON LONGITUDINAL STRESSES AT MIDSHIP SECTION FOR SYMMETRICAL TEMPERATURE DISTRIBUTION COMPUTER SOLUTION.

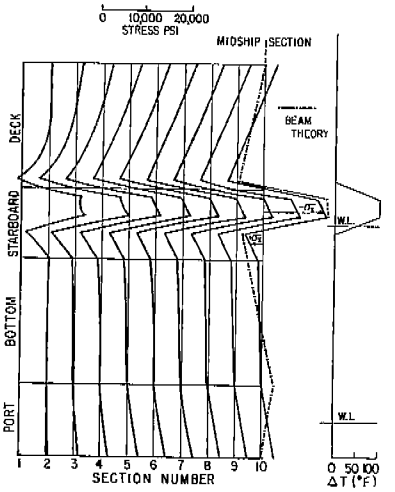

FIG. 45. LONGITUDINAL STRESSES FOR ASYMMETRICAL TEMPERATURE DISTRIBUTION, COMPUTER SOLUTION.

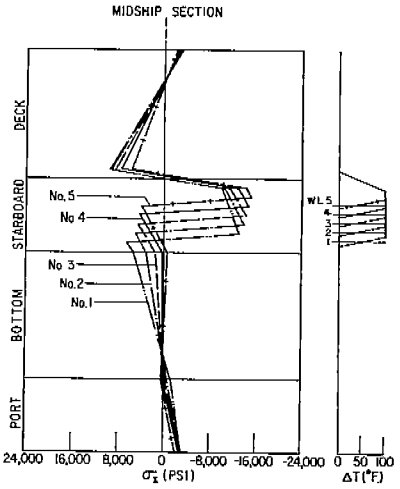

FIG. 46. EFFECT OF DRAFT ON LONGITUDINAL STRESSES AT MIDSHIP SECTION FOR ASYMMETRICAL TEMPERATURE DISTRIBUTION, COMPUTER SOLUTION.

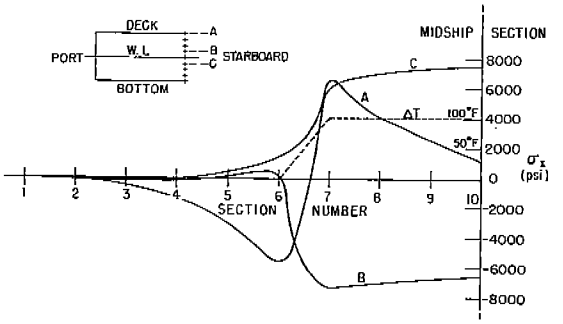

FIG. 48. EFFECT OF LONGITUDINAL TEMPERATURE GRADIENT ON LONGITUDINAL STRESS.

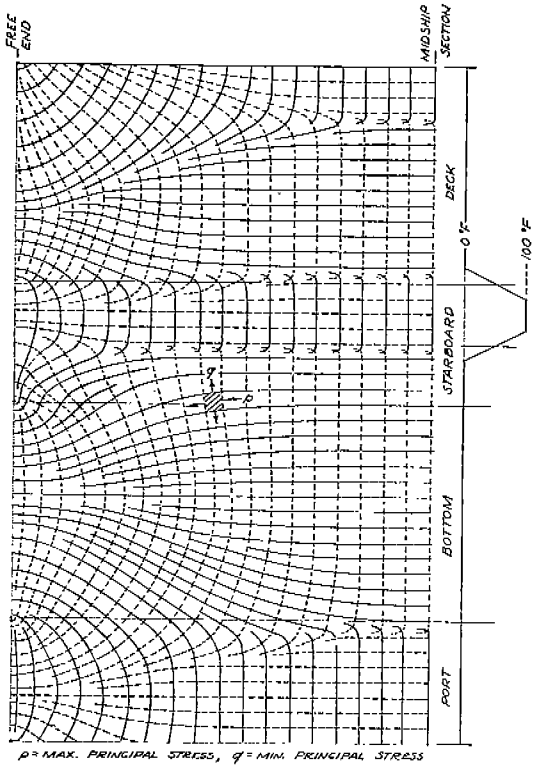

FIG. 47. PRINCIPAL STRESSES -- ASYMMETRICAL TEMPERATURE.

The strain-displacement equation

$$e_Y = \frac{\partial v}{\partial y} = 0 \tag{28}$$

states the condition that the transverse strain is zero everywhere along the fixed end at x = const. Application of the stress-strain law in terms of the Airy stress function yields

$$e_Y = \frac{1}{E}\frac{\partial^2 \varphi}{\partial x^2} - \nu \frac{1}{E}\frac{\partial^2 \varphi}{\partial y^2} + \alpha T = 0 \tag{29}$$

or

$$\frac{\partial^2 \varphi}{\partial x^2} - \nu \frac{\partial^2 \varphi}{\partial y^2} + E\alpha T = 0 \tag{30}$$

Equation 30 represents one of the two necessary conditions which must be satisfied along the fixed end, x = const. The second condition to be satisfied may be found by consideration of the following strain-displacement equation

$$\gamma_{xy} = \frac{\partial u}{\partial y} + \frac{\partial v}{\partial x} \tag{31}$$

Since the longitudinal displacement is assumed zero everywhere along x = const., it follows that the derivative of the longitudinal displacement with respect to the transverse coordinate v must be equal to zero, therefore

$$\gamma_{xy} = \frac{\partial v}{\partial x} \tag{32}$$

If the derivative of this last expression is taken with respect to the transverse coordinate y it is possible to write this expression in terms of the Airy stress function as follows

$$\frac{\partial \gamma_{xy}}{\partial y} = \frac{\partial}{\partial x}\left(\frac{\partial v}{\partial y}\right)$$

or

$$\frac{1}{G}\frac{\partial}{\partial y}\left(-\frac{\partial^2 \varphi}{\partial x \partial y}\right) = \frac{\partial}{\partial x}\left(\frac{1}{E}\frac{\partial^2 \varphi}{\partial x^2} - \frac{\nu}{E}\frac{\partial^2 \varphi}{\partial y^2} + \alpha T\right)$$

which finally reduces to

$$(2+\nu)\frac{\partial^3 \varphi}{\partial x \partial y^2} + \frac{\partial^3 \varphi}{\partial x^3} + E\alpha\frac{\partial T}{\partial x} = 0 \tag{33}$$

Now Eqs. 30 and 33 represent the displacement conditions to be satisfied along the fixed edge x = const. in terms of the Airy stress function.

Equations 30 and 33 were expressed in finite-difference form and incorporated into the computer program previously discussed. The resulting stresses in the flat-plate model with rigidly constrained ends appeared generally to represent a distribution which one might anticipate. However, beginning at the extreme ends of the line of constraint (x = const.) there appeared a perturbation in the computed stresses which damped out toward the center of the plate. Numerous checks have been made on the correctness of the formulation, but no improvement in the accuracy of the solution could be established. Further question on the adequacy of the solution was raised by failure to check the overall equilibrium of the plate by a factor of the order of 10 per cent.

Although the questions which these attempted solutions have raised are still unanswered, it does appear that the problem resides with the added difficulty of expressing the boundary conditions in a region of rapid change in stresses through finite-difference relations where third rather than first derivations of the stress functions are involved. This situation arises by virtue of the mixed boundary conditions (same stress and others displacement). It would appear, then, that a much finer mesh and/or a different formulation of the basic computer program are necessary. It may be, however, that the results obtained are closer to the actual values than supposed, but verification must await guaranteed refinement of the solution.

This problem of a restraining line in a flat plate should be solved satisfactorily at some future time before any attempts are made to handle the folded-plate girder.

EXTENSION TO CROSS STIFFENED PLATING

To modify the elastic beam solution to account for the presence of stiffened plate construction, it is only necessary to introduce a new set of stress-strain laws. The othogonal properties of this type of construction will require the use and determination of four elastic constants.

$$e_X = \frac{\sigma_X}{E_X} - \frac{\sigma_Y}{E_{XY}} + \alpha T \tag{34}$$

$$e_Y = \frac{\sigma_Y}{E_Y} - \frac{\sigma_X}{E_{XY}} + \alpha T$$

$$\gamma_{XY} = \tau_{XY}/G.$$

The elastic constants introduced in the above equations are defined by the use in these equations. The Airy stress function is defined in the usual manner, and substituted into the stress-strain equations. These stress-strain equations are now substituted into the compatibility equation to get

$$\frac{\partial^4\varphi}{\partial x^4} + 2\left(\frac{E_X}{2G} - \frac{E_X}{E_{XY}}\right)\frac{\partial^4\varphi}{\partial x^2\partial y^2} + \frac{E_X}{E_Y}\frac{\partial^4\varphi}{\partial y^4} + E_X\alpha\nabla^2 T \qquad (35)$$

It is seen that the above equation reduces to Eq. (11) when the material constants for an isotropic material are used. The finite-difference expression for Eq. (35) is given as follows

$$[2\rho^2(3\beta_1\rho^2 + 4\beta_2) + 6]\varphi_0 - 4[1 + 4\beta_2\rho^2](\varphi_1 + \varphi_3) - 4\rho^2(\beta_1\rho^2 + \beta_2)(\varphi_2 + \varphi_4) + 2\beta_2\rho^2(\varphi_5 + \varphi_6 + \varphi_7 + \varphi_8) + (\varphi_9 + \varphi_{11}) + \beta_1\rho^4(\varphi_{10} + \varphi_{12}) + \rho^2 E\alpha[(T_1 + T_3) + \rho^2(T_2 + T_4) - 2(\rho^2 + 1)T_0] = 0 \qquad (36)$$

where

$$\beta_1 = \frac{E_X}{E_Y}$$

$$\beta_2 = \frac{E_X}{2G} - \frac{E_X}{E_{XY}}$$

The use of the above equations will not give the stress distribution for discrete stiffening but will give usable results for averaged stiffening. The major difficulty with application of these equations is the determination of the four elastic constants, as is the case in any nonisotropic elastic problem. It is most probable that model tests would be necessary to determine appropriate elastic constants for any given structural configuration before numerical studies could be conducted.

EXTENSION TO PLATING OF VARIABLE THICKNESS

To modify the elastic beam solution to account for the presence of variable plating thickness, a dimensionless reciprocal thickness H is introduced into the equations of equilibrium.

$$\left.\begin{aligned}\frac{\partial(\sigma_X/H)}{\partial x} + \frac{\partial(\tau_{XY}/H)}{\partial y} &= 0\\ \frac{\partial(\tau_{XY}/H)}{\partial x} + \frac{\partial(\sigma_Y/H)}{\partial y} &= 0\end{aligned}\right\} \qquad (37)$$

To satisfy these equations a stress function is introduced as

$$\left.\begin{aligned}\sigma_X &= H\frac{\partial^2\varphi}{\partial y^2}\\ \sigma_Y &= H\frac{\partial^2\varphi}{\partial x^2}\\ \tau_{XY} &= -H\frac{\partial^2\varphi}{\partial x\partial y}\end{aligned}\right\} \qquad (38)$$

Introduction of this stress function into the isotropic stress-strain law and application of the compatibility equation yield the following equation

$$\nabla^4\varphi + \xi_1\frac{\partial^2\varphi}{\partial x^2} + \xi_2\frac{\partial^2\varphi}{\partial y^2} + \xi_3\frac{\partial^2\varphi}{\partial x\partial y} + \frac{E\alpha}{H}\nabla^2 T \qquad (39)$$

where

$$\xi_1 = \left[\frac{\partial^2 H}{\partial x^2} - \nu\frac{\partial^2 H}{\partial y^2}\right]\frac{1}{H}$$

$$\xi_2 = \left[\frac{\partial^2 H}{\partial y^2} - \nu\frac{\partial^2 H}{\partial x^2}\right]\frac{1}{H}$$

$$\xi_3 = \left[2(1+\nu)\frac{\partial^2 H}{\partial x\,\partial y}\right]\frac{1}{H}$$

The finite difference expression for Eq. (39) using a rectangular mesh with length to height ratio of ρ is given by

$$[6(1+\rho^4)+8\rho^2-2\rho^2(\xi_1+\rho^2\xi_2)]\varphi_0 -$$

$$(4-\rho^2\xi_1)(\varphi_1+\varphi_3)-\rho^4(4-\xi_2)(\varphi_2+\varphi_4)+$$

$$\frac{\rho^3\xi_3}{4}(\varphi_5+\varphi_7-\varphi_6-\varphi_8)+(\varphi_9+\varphi_{11})+$$

$$\rho^4(\varphi_{10}+\varphi_{12})+2\rho^2\Sigma\varphi_5-4\rho^2\Sigma\varphi_1+$$

$$\rho^2\frac{E\alpha}{H}[(T_1+T_3)+\rho^2(T_2+T_4)-$$

$$2(1+\rho^2)T_0]=0 \qquad (40)$$

where

$$\xi_1=\left[\left(\frac{H_1+H_3-2H_0}{\rho^2}\right)-\nu(H_2+H_4-2H_0)\right]\frac{1}{H_0}$$

$$\xi_2=\left[(H_2+H_4-2H_0)-\nu\left(\frac{H_1+H_3-2H_0}{\rho^2}\right)\right]\frac{1}{H_0}$$

$$\xi_3=\left[2(1+\nu)\left(\frac{H_5+H_7-H_6-H_8}{4\rho}\right)\right]\frac{1}{H_0}$$

Although Eq. (40) seems quite formidable at first sight, it must be remembered that E, α, ν, ρ and H are all known at the outset of the problem, and hence enter only as parameters in the set of equations to be solved. The setting up of these equations is, of course, best handled by a computer program.

DISCUSSION, CONCLUSIONS, AND RECOMMENDATIONS

Experimental. The experimental results justify the following statements:

(1) The generally good agreement between measured and computed longitudinal thermal stresses in the model and the reproducibility of results indicates that the facilities and instrumentation developed for this study were adequate for the measurement of stress and temperature.

(2) This good agreement indicates clearly that the center section of the model behaves as a beam within the strength-of-materials limitations. Therefore, the strength-of-materials solution, Eq. (9) and (10), is a valid design prediction in the absence of transverse restraint and without longitudinal temperature gradients. This conclusion verifies the simular conclusion tentatively drawn from the SS Boulder Victory tests.[1]

(3) The environmental control for the model and the thermocouple installation proved to be insufficient to permit the control and measurement of longitudinal temperature gradients needed to obtain corresponding stresses. Experience showed that a very extensive thermocouple mapping of essentially the entire half model or more would have to be provided in order to determine enough information on the longitudinal temperature gradients to permit significant interpretation of stress measurements. Such extensive mapping was not feasible in the present test program. Furthermore, a much more elaborate means of local temperature excitation and control would have to be provided in order to permit significant measurements of longitudinal effects. One inconsistency between calculated and experimental results for a section of the deck was due, it was felt, to a slight nonuniformity in longitudinal temperature which persisted by virtue of a nonuniformity in heat flow.

(4) Accumulated experience with the model test results plus strong indication from the theoretical calculations of the localized nature of the end effects justified the decision not to attach end sections to the model.

(5) The reliable measurement of transverse restraint effects proved to be difficult, due in part to the uncertainty of localized temperature gradients disturbed by heat transfer to the restraining bulkhead. Also it was difficult to interpret strains in the neighborhood of the abrupt change in geometry introduced by the bulkhead. It appears that these changes are more localized than were anticipated.

(6) Precise temperature compensation for the strain gage circuits requires an accurate calibration of apparent strain versus temperature which should be measured under the condition of the test insofar as possible rather than obtained from manufacturer's published calibration.

Theoretical. The theoretical calculations justify the following statements:

(1) The use of the finite-difference method of solution in conjunction with the availability of a high-speed digital computer has been demonstrated as a highly adequate method of solving the thermal stress problem in strips

and beams.

(2) It has been shown that the determination of the accuracy of the solution may be easily established by a variation in the finite-difference mesh size.

(3) For all of the temperature distributions studied, the end effect in the two-dimensional strip is confined to a region at the end of the strip whose length is approximately equal to the width of the strip.

(4) In the absence of longitudinal temperature gradients the strength-of-materials solution agrees, for all practical purposes, exactly with the elastic solution for the two-dimensional strip except in the end-effect region.

(5) The solution to the general thermal stress problem in the box beam represented as a combination of plane-stress elements, has been demonstrated.

(6) For the elastic box beam, as in the case of the strip, the end effect is confined to a region which extends a distance into the end of the beam approximately equal to the maximum width of the beam.

(7) When the elastic box beam is subjected to symmetrical transverse temperature distributions, the agreement between the elastic solution and the strength-of-materials solution is for all practical purposes exact, except at the ends of the beam.

(8) When the elastic box beam is subjected to asymmetrical transverse temperature distributions, the elastic solution does not agree with the strength-of-materials solution. This disagreement, while never very large, appears to be due to warpage of the cross section. This type of distortion is permitted in the elastic box beam but not in the strength-of-materials solution. In spite of these differences, the elastic solution and the strength-of-materials solution agree quite well in the regions of peak stress.

(9) It is strongly recommended that the ship designer be clearly aware of the regions of critical thermal stresses. These regions of critical thermal stresses will always occur at those points at which temperature distributions become nonlinear. The more abrupt the departure from linearity, the more critical the thermal stress. Critical areas for thermal stresses in ships normally occur at places such as the waterline, at shadow boundaries on the deck and sides, and at boundaries between various tanks or compartments. In most cases the designer has no control over the environment which gives rise to the nonlinear temperature distributions, and for that matter the operator seldom has much control over the environment either. So it appears that the designer is mainly concerned with the ability to live with whatever thermal stresses may be present in the structure. In some cases the critical thermal stresses occur in areas where the nominal stress level is quite low. For instance the stress level in the vicinity of the waterline due to bending loads is quite small. However peak thermal stresses which can arise in the deck may superimpose with bending stresses to create dangerous situations.

ACKNOWLEDGMENTS

The authors wish to acknowledge, first, the interest of the Committee on Ship Structural Design of the National Academy of Sciences and the support of the Ship Structure Committee during the course of this investigation. The detailed interest and guidance of the Project Advisory Committee under the chairmanship of Professor William Prager is especially appreciated.

The project was fortunate to have the services of Mr. Hong Liu and Mr. Martin Ewolsen, graduate students in engineering, on a part-time basis to help with the instrumentation, and the taking and plotting of data. Each made important contributions. Special praise goes to Mr. Herman Werner whose expert welding enabled the construction of a model, the accuracy of which would be hard to excel.

NOMENCLATURE

x, y, z	Cartesean Coordinates
n	Normal Coordinates
u, v	Elastic Displacements
e	Elastic Strain

$\bar{e}$	Total Strain
γ	Shear Strain
δ	Elongation
L, ℓ	Length
A	Cross Section Area
I	Second Moment of Area
E	Elastic Modulus
G	Shear Modulus
ν	Poisson's Ratio
α	Longitudinal Coefficient of Expansion
T	Temperature Change
φ	Airy Stress Function
f, g	General Functions
x, y	General Functions
∇^2	Laplacian Operator
∇^4	Biharmonic Operator
C_1, C_2, C_3	Constants of Integration
x, y, z	Directional Subscripts
1, 2	Directional Subscripts
1, 2	Element Subscripts
m, p	Subscript Denoting Model or Prototype

REFERENCES

1. Meriam, J. L., Lyman, P. T., Steidel, R. F., and Brown, G. W., "Thermal Stresses in the SS BOULDER VICTORY", Report to S-10 Panel, Society of Naval Architects and Marine Engineers, (Institute of Engineering Research, University of California, Berkeley, Series 101, Issue 3, October 4, 1957) also Journal of Ship Research, vol. 2, October 1958.

2. Jasper, N. H., "Temperature Induced Stresses in Beams and Ships", DTMB Report 937, David Taylor Model Basin, Washington, June 1955.

3. International Business Machines Corporation Reference Manual 704 FORTRAN Programming System.

4. Timoshenko, S., and Goodier, J. N., Theory of Elasticity; McGraw-Hill Book Co., Inc., 1951.

5. Lyman, P. T., "Thermal Stresses in Ships", Dissertation submitted in partial fulfillment for the degree of Doctor of Engineering, University of California, Berkeley, December 1962.

6. Salvadori, M. G., and Baron, M. L., Numerical Methods in Engineering, Prentice Hall, Inc., 1961.

7. Crandall, S. H., Engineering Analysis: A Survey of Numerical Procedures, McGraw-Hill Book Co. Inc., 1956.

8. Hildebrand, F. B., Introduction to Numerical Analysis, McGraw-Hill Book Co., Inc., 1956.

9. Dwyer, P. S., Linear Computation, John Wiley & Sons, Inc., 1951.

10. Aitken, A. C., "The Evaluation of the Latent Roots and Latent Vectors of a Matrix", Proc. Royal Society, Edinburgh, vol. 57, pp. 269-304, 1937.

11. Heldenfels, R. R., and Roberts, W. M., Experimental and Theoretical Determination of Thermal Stresses in Flat Plates, (NACA TN-2769), National Advisory Committee for Aeronautics, Aug. 1952.

12. Horvay, G., "The End Effects of Rectangular Strips", Journal of Applied Mechanics, vol. 75, pp. 87-94, 1953.

13. Crout, G. P. D., "A Short Method for Evaluating Determinates and Solving Systems of Linear Equations with Real or Complex Coefficients", Marchant Methods, MM-182, Sept. 1941, Marchant Calculating Machine Co., Oakland, Calif.

APPENDIX A - TABULAR RESULTS CORRESPONDING TO GRAPHICAL RESULTS PRESENTED IN FIGS. 38 THROUGH 43 AND FIG. 47.

DECK STRESS 360 ELEMENT MODEL TEMPERATURE DISTRIBUTION A100

ROW	COL	XX-STRESS PSI	YY-STRESS PSI	XY-STRESS PSI	MAX-STRESS PSI	MIN-STRESS PSI	SHEAR STRESS PSI	DIRECTION DEG
1	1	0.	0.	0.	0.	0.	0.	ISOTROPIC POINT
2	1	0.	-449.90	0.	-0.	-449.90	224.95	0.
3	1	0.	-708.90	0.	-0.	-708.90	354.45	0.
4	1	0.	-854.16	0.	-0.	-854.16	427.08	0.
5	1	0.	-932.88	0.	-0.	-932.88	466.44	0.
6	1	0.	-973.41	0.	-0.	-973.41	486.71	0.
7	1	0.	-992.16	0.	-0.	-992.16	496.08	0.
8	1	0.	-997.54	0.	-0.	-997.54	498.77	0.
9	1	0.	-992.16	0.	-0.	-992.16	496.08	0.
10	1	0.	-973.41	0.	-0.	-973.41	486.71	0.
11	1	0.	-932.88	0.	-0.	-932.88	466.44	0.
12	1	0.	-854.16	0.	-0.00	-854.16	427.08	0.
13	1	0.	-708.90	0.	-0.	-708.90	354.45	0.
14	1	0.	-449.90	0.	-0.	-449.90	224.95	0.
15	1	0.	0.	0.	0.	0.	0.	ISOTROPIC POINT
1	2	1421.16	0.	689.87	1700.96	-279.79	990.38	22.08
2	2	859.04	62.45	497.90	1098.35	-176.86	637.61	25.67
3	2	511.83	45.03	352.04	700.81	-143.95	422.38	28.23
4	2	299.46	-2.67	242.63	434.21	-137.42	285.81	29.05
5	2	171.80	-54.50	160.38	254.93	-137.63	196.28	27.40
6	2	98.07	-97.26	97.09	138.12	-137.30	137.71	22.42
7	2	60.12	-124.66	45.69	70.80	-135.34	103.07	13.16
8	2	48.45	-134.04	0.00	48.45	-134.04	91.25	0.00
9	2	60.12	-124.66	-45.68	70.80	-135.34	103.07	-13.16
10	2	98.07	-97.26	-97.09	138.12	-137.30	137.71	-22.41
11	2	171.80	-54.50	-160.38	254.93	-137.63	196.28	-27.40
12	2	299.46	-2.67	-242.63	434.21	-137.42	285.81	-29.05
13	2	511.83	45.03	-352.04	700.81	-143.95	422.38	-28.23
14	2	859.04	62.45	-497.90	1098.35	-176.86	637.61	-25.67
15	2	1421.16	0.	-689.87	1700.96	-279.79	990.38	-22.08
1	3	1304.38	0.	337.02	1386.31	-81.93	734.12	13.66
2	3	999.24	78.18	366.17	1127.08	-49.65	588.36	19.24
3	3	751.14	130.60	338.97	900.40	-18.66	459.53	23.77
4	3	561.72	160.71	283.83	708.72	13.71	347.50	27.38
5	3	425.25	175.20	216.44	550.18	50.27	249.95	29.99
6	3	334.31	180.56	144.79	421.37	93.50	163.93	31.02
7	3	282.51	181.76	72.33	320.27	144.00	88.14	27.57
8	3	265.71	181.83	-0.00	265.71	181.83	41.94	-0.00
9	3	282.51	181.76	-72.33	320.27	144.00	88.14	-27.57
10	3	334.31	180.56	-144.79	421.37	93.50	163.93	-31.02
11	3	425.25	175.20	-216.44	550.18	50.28	249.95	-29.99
12	3	561.72	160.71	-283.83	708.72	13.71	347.50	-27.38
13	3	751.14	130.60	-338.97	900.40	-18.66	459.53	-23.77
14	3	999.25	78.18	-366.17	1127.08	-49.65	588.36	-19.24
15	3	1304.38	0.	-337.02	1386.31	-81.93	734.12	-13.66
1	4	1022.77	0.	149.21	1044.10	-21.32	532.71	8.13
2	4	907.58	44.40	201.10	952.13	-0.15	476.14	12.49
3	4	789.68	89.50	213.80	849.81	29.38	410.22	15.71
4	4	683.38	128.77	197.90	746.75	65.39	340.68	17.76
5	4	596.55	159.47	162.39	650.28	105.74	272.27	18.31
6	4	533.10	180.98	114.28	566.93	147.15	209.89	16.49
7	4	494.67	193.59	58.82	505.75	182.51	161.62	10.67
8	4	481.82	197.73	-0.00	481.82	197.73	142.04	-0.00
9	4	494.67	193.59	-58.82	505.75	182.51	161.62	-10.67
10	4	533.10	180.98	-114.28	566.93	147.15	209.89	-16.49
11	4	596.54	159.47	-162.39	650.27	105.74	272.26	-18.31
12	4	683.38	128.77	-197.90	746.75	65.39	340.68	-17.76
13	4	789.69	89.50	-213.80	849.81	29.38	410.22	-15.71
14	4	907.58	44.40	-201.10	952.13	-0.15	476.14	-12.49
15	4	1022.78	0.	-149.21	1044.10	-21.32	532.71	-8.13
1	5	858.81	0.	66.35	863.90	-5.10	434.50	4.39
2	5	822.18	22.37	97.18	833.82	10.73	411.55	6.83
3	5	775.77	49.07	110.60	792.23	32.61	379.81	8.46
4	5	727.96	75.61	108.12	745.41	58.15	343.63	9.17
5	5	685.12	98.79	92.53	699.38	84.53	307.42	8.76
6	5	651.72	116.53	67.09	660.00	108.25	275.88	7.04
7	5	630.62	127.59	35.15	633.07	125.15	253.96	3.98
8	5	623.42	131.34	0.00	623.42	131.34	246.04	0.00
9	5	630.62	127.59	-35.15	633.07	125.15	253.96	-3.98
10	5	651.72	116.53	-67.09	660.00	108.25	275.88	-7.04
11	5	685.12	98.79	-92.53	699.38	84.53	307.42	-8.76
12	5	727.96	75.61	-108.12	745.42	58.15	343.63	-9.17
13	5	775.77	49.06	-110.60	792.23	32.61	379.81	-8.46
14	5	822.19	22.37	-97.18	833.82	10.73	411.55	-6.83
15	5	858.81	0.	-66.35	863.91	-5.10	434.50	-4.39

DECK STRESS 360 ELEMENT MODEL TEMPERATURE DISTRIBUTION A100

ROW	COL	XX-STRESS PSI	YY-STRESS PSI	XY-STRESS PSI	MAX-STRESS PSI	MIN-STRESS PSI	SHEAR STRESS PSI	DIRECTION DEG
1	6	784.65	0.	28.24	785.67	-1.02	393.34	2.06
2	6	775.76	10.54	42.40	778.10	8.19	384.95	3.16
3	6	760.43	23.97	49.98	763.81	20.59	371.61	3.86
4	6	742.34	38.13	50.45	745.93	34.54	355.70	4.08
5	6	724.72	51.15	44.31	727.63	48.24	339.69	3.75
6	6	710.23	61.50	32.74	711.88	59.85	326.01	2.88
7	6	700.78	68.14	17.35	701.25	67.66	316.80	1.57
8	6	697.50	70.42	0.00	697.50	70.42	313.54	0.00
9	6	700.78	68.14	-17.35	701.25	67.66	316.80	-1.57
10	6	710.24	61.50	-32.74	711.88	59.85	326.01	-2.88
11	6	724.72	51.15	-44.31	727.62	48.24	339.69	-3.75
12	6	742.34	38.13	-50.45	745.93	34.54	355.70	-4.08
13	6	760.44	23.97	-49.98	763.81	20.59	371.61	-3.86
14	6	775.76	10.54	-42.40	778.10	8.19	384.95	-3.16
15	6	784.65	0.	-28.24	785.67	-1.02	393.34	-2.06
1	7	755.74	0.	10.99	755.90	-0.16	378.03	0.83
2	7	755.34	4.55	16.54	755.71	4.19	375.76	1.26
3	7	751.75	10.53	19.92	752.29	9.99	371.15	1.54
4	7	746.33	17.03	20.57	746.91	16.45	365.23	1.61
5	7	740.42	23.18	18.42	740.89	22.71	359.09	1.47
6	7	735.24	28.18	13.80	735.51	27.91	353.80	1.12
7	7	731.75	31.44	7.38	731.83	31.36	350.23	0.60
8	7	730.52	32.57	-0.00	730.52	32.57	348.97	-0.00
9	7	731.75	31.44	-7.38	731.83	31.36	350.23	-0.60
10	7	735.25	28.19	-13.80	735.52	27.92	353.80	-1.12
11	7	740.42	23.18	-18.42	740.89	22.71	359.09	-1.47
12	7	746.33	17.03	-20.57	746.91	16.45	365.23	-1.61
13	7	751.76	10.53	-19.92	752.29	9.99	371.15	-1.54
14	7	755.34	4.55	-16.54	755.71	4.19	375.76	-1.26
15	7	755.74	0.	-10.99	755.90	-0.16	378.03	-0.83
1	8	746.18	0.	3.75	746.20	-0.02	373.11	0.29
2	8	747.70	1.74	5.58	747.74	1.70	373.02	0.43
3	8	747.87	4.07	6.86	747.94	4.01	371.96	0.53
4	8	747.09	6.67	7.25	747.16	6.60	370.28	0.56
5	8	745.82	9.18	6.61	745.88	9.13	368.38	0.51
6	8	744.52	11.26	5.02	744.55	11.23	366.66	0.39
7	8	743.58	12.63	2.71	743.59	12.62	365.48	0.21
8	8	743.24	13.11	-0.00	743.24	13.11	365.06	-0.00
9	8	743.58	12.63	-2.71	743.59	12.62	365.48	-0.21
10	8	744.52	11.26	-5.02	744.55	11.23	366.66	-0.39
11	8	745.82	9.18	-6.61	745.88	9.13	368.38	-0.51
12	8	747.09	6.67	-7.25	747.16	6.60	370.28	-0.56
13	8	747.87	4.07	-6.86	747.94	4.01	371.96	-0.53
14	8	747.70	1.74	-5.58	747.75	1.70	373.02	-0.43
15	8	746.18	0.	-3.75	746.20	-0.02	373.11	-0.29
1	9	743.71	0.	1.03	743.71	-0.00	371.86	0.08
2	9	745.32	0.58	1.51	745.33	0.57	372.38	0.12
3	9	746.42	1.37	1.89	746.43	1.36	372.53	0.15
4	9	747.06	2.28	2.05	747.06	2.27	372.40	0.16
5	9	747.33	3.18	1.91	747.34	3.18	372.08	0.15
6	9	747.40	3.95	1.47	747.40	3.95	371.73	0.11
7	9	747.38	4.46	0.80	747.38	4.46	371.46	0.06
8	9	747.36	4.64	0.00	747.36	4.64	371.36	0.00
9	9	747.38	4.46	-0.80	747.38	4.46	371.46	-0.06
10	9	747.40	3.95	-1.47	747.40	3.95	371.73	-0.11
11	9	747.33	3.18	-1.91	747.34	3.18	372.08	-0.15
12	9	747.05	2.27	-2.05	747.06	2.27	372.39	-0.16
13	9	746.42	1.36	-1.89	746.43	1.36	372.53	-0.15
14	9	745.33	0.58	-1.50	745.33	0.57	372.38	-0.12
15	9	743.71	0.	-1.03	743.71	-0.00	371.86	-0.08
1	10	743.32	0.	0.	743.32	0.	371.66	0.
2	10	744.84	0.27	0.	744.84	0.27	372.29	0.
3	10	746.07	0.64	0.	746.07	0.64	372.72	0.
4	10	746.99	1.09	0.	746.99	1.09	372.95	0.
5	10	747.61	1.56	0.	747.61	1.56	373.02	0.
6	10	747.99	1.97	0.	747.99	1.97	373.01	0.
7	10	748.18	2.24	0.	748.18	2.24	372.97	0.
8	10	748.24	2.34	0.	748.24	2.34	372.95	0.
9	10	748.19	2.24	0.	748.19	2.24	372.97	0.
10	10	747.99	1.97	0.	747.99	1.97	373.01	0.
11	10	747.60	1.56	0.	747.60	1.56	373.02	0.
12	10	746.99	1.09	0.	746.99	1.09	372.95	0.
13	10	746.07	0.64	0.	746.07	0.64	372.72	0.
14	10	744.84	0.27	0.	744.84	0.27	372.29	0.
15	10	743.33	0.	0.	743.33	0.	371.66	0.

STBD STRESS 360 ELEMENT MODEL TEMPERATURE DISTRIBUTION AIOO

ROW	COL	XX-STRESS PSI	YY-STRESS PSI	XY-STRESS PSI	MAX-STRESS PSI	MIN-STRESS PSI	SHEAR STRESS PSI	DIRECTION DEG
1	1	0.	0.	0.	0.	0.	0.	ISOTROPIC POINT
2	1	0.	765.71	0.	765.71	0.	382.86	90.00
3	1	0.	1377.53	0.	1377.53	0.	688.76	90.00
4	1	0.	1336.10	0.	1336.10	0.	668.05	90.00
5	1	0.	0.00	0.	0.00	0.	0.00	90.00
6	1	0.	-1336.09	0.	-0.	-1336.09	668.05	0.
7	1	0.	-1377.52	0.	-0.	-1377.52	688.76	0.
8	1	0.	-765.71	0.	-0.	-765.71	382.86	0.
9	1	0.	0.	0.	0.	0.	0.	ISOTROPIC POINT
1	2	1421.16	0.	-689.87	1700.96	-279.79	990.38	-22.08
2	2	-692.55	-233.34	-685.82	260.29	-1186.18	723.24	-54.25
3	2	-2939.61	-463.10	-233.39	-441.30	-2961.41	1260.06	-84.66
4	2	-5825.98	-492.53	685.82	-405.75	-5912.75	2753.50	82.79
5	2	-0.00	-0.00	1265.35	1265.35	-1265.35	1265.35	45.00
6	2	5825.97	492.53	685.82	5912.75	405.75	2753.50	7.21
7	2	2939.61	463.10	-233.39	2961.41	441.30	1260.06	-5.34
8	2	692.55	233.34	-685.82	1186.18	-260.29	723.23	-35.74
9	2	-1421.16	0.	-689.87	279.79	-1700.96	990.37	-67.92
1	3	1304.38	0.	-337.02	1386.31	-81.93	734.12	-13.66
2	3	-1352.95	-96.50	-221.46	-58.60	-1390.84	666.12	-80.29
3	3	-4076.19	-156.05	-15.85	-155.99	-4076.25	1960.13	-89.77
4	3	-6954.37	-127.36	221.46	-120.18	-6961.54	3420.68	88.14
5	3	-0.00	-0.00	335.53	335.52	-335.53	335.53	45.00
6	3	6954.36	127.36	221.46	6961.53	120.18	3420.68	1.86
7	3	4076.19	156.05	-15.85	4076.25	155.99	1960.13	-0.23
8	3	1352.95	96.49	-221.46	1390.84	58.60	666.12	-9.71
9	3	-1304.38	0.	-337.02	81.93	-1386.31	734.12	-76.34
1	4	1022.78	0.	-149.21	1044.10	-21.32	532.71	-8.13
2	4	-1680.93	-31.33	-72.03	-28.19	-1684.07	827.94	-87.50
3	4	-4418.47	-43.18	6.97	-43.17	-4418.48	2187.65	89.91
4	4	-7194.82	-30.90	72.03	-30.18	-7195.54	3582.68	89.42
5	4	-0.00	0.00	98.14	98.14	-98.14	98.14	45.00
6	4	7194.81	30.90	72.03	7195.54	30.18	3582.68	0.58
7	4	4418.46	43.18	6.97	4418.48	43.17	2187.65	0.09
8	4	1680.93	31.33	-72.03	1684.07	28.19	827.94	-2.50
9	4	-1022.78	0.	-149.21	21.32	-1044.10	532.71	-81.87
1	5	858.81	0.	-66.35	863.91	-5.10	434.50	-4.39
2	5	-1833.60	-12.39	-28.15	-11.95	-1834.03	911.04	-89.11
3	5	-4543.57	-15.32	4.96	-15.32	-4543.57	2264.13	89.94
4	5	-7267.67	-10.13	28.15	-10.02	-7267.78	3628.88	89.78
5	5	-0.00	-0.00	36.59	36.59	-36.59	36.59	45.00
6	5	7267.67	10.13	28.15	7267.78	10.02	3628.88	0.22
7	5	4543.56	15.32	4.96	4543.57	15.32	2264.13	0.06
8	5	1833.60	12.39	-28.15	1834.03	11.95	911.04	-0.89
9	5	-858.81	0.	-66.35	5.10	-863.91	434.50	-85.61
1	6	784.65	0.	-28.24	785.67	-1.02	393.34	-2.06
2	6	-1901.18	-5.51	-11.73	-5.44	-1901.26	947.91	-89.65
3	6	-4595.51	-6.57	2.29	-6.56	-4595.51	2294.47	89.97
4	6	-7296.08	-4.22	11.73	-4.20	-7296.10	3645.95	89.91
5	6	-0.00	0.00	15.07	15.07	-15.07	15.07	45.00
6	6	7296.08	4.22	11.73	7296.10	4.20	3645.95	0.09
7	6	4595.51	6.57	2.29	4595.51	6.56	2294.47	0.03
8	6	1901.18	5.51	-11.73	1901.26	5.44	947.91	-0.35
9	6	-784.65	0.	-28.25	1.02	-785.67	393.34	-87.94
1	7	755.74	0.	-10.99	755.90	-0.16	378.03	-0.83
2	7	-1928.68	-2.40	-4.67	-2.39	-1928.69	963.15	-89.86
3	7	-4616.81	-2.85	0.89	-2.85	-4616.81	2306.98	89.99
4	7	-7307.68	-1.82	4.67	-1.82	-7307.69	3652.93	89.96
5	7	-0.00	0.00	6.00	6.00	-6.01	6.00	45.01
6	7	7307.68	1.83	4.67	7307.68	1.82	3652.93	0.04
7	7	4616.81	2.85	0.89	4616.81	2.85	2306.98	0.01
8	7	1928.68	2.40	-4.67	1928.69	2.39	963.15	-0.14
9	7	-755.74	0.	-10.99	0.16	-755.90	378.03	-89.17
1	8	746.18	0.	-3.75	746.20	-0.02	373.11	-0.29
2	8	-1938.59	-0.96	-1.67	-0.96	-1938.59	968.82	-89.95
3	8	-4624.81	-1.15	0.29	-1.15	-4624.81	2311.83	90.00
4	8	-7312.11	-0.74	1.67	-0.74	-7312.11	3655.69	89.99
5	8	-0.00	0.00	2.16	2.16	-2.16	2.16	45.02
6	8	7312.11	0.74	1.67	7312.11	0.74	3655.69	0.01
7	8	4624.81	1.15	0.29	4624.81	1.15	2311.83	0.00
8	8	1938.59	0.96	-1.67	1938.60	0.96	968.82	-0.05
9	8	-746.18	0.	-3.75	0.02	-746.20	373.11	-89.71
1	9	743.71	0.	-1.03	743.71	-0.00	371.86	-0.08
2	9	-1941.60	-0.35	-0.49	-0.35	-1941.60	970.63	-89.99
3	9	-4627.40	-0.42	0.07	-0.42	-4627.40	2313.49	90.00
4	9	-7313.60	-0.28	0.49	-0.28	-7313.60	3656.66	90.00
5	9	-0.00	-0.00	0.64	0.64	-0.64	0.64	45.09
6	9	7313.59	0.28	0.49	7313.59	0.28	3656.66	0.00
7	9	4627.40	0.42	0.08	4627.40	0.42	2313.49	0.00
8	9	1941.60	0.35	-0.49	1941.60	0.35	970.63	-0.01
9	9	-743.71	0.	-1.03	0.00	-743.71	371.85	-89.92
1	10	743.33	0.	0.	743.33	0.	371.66	0.
2	10	-1942.20	-0.18	0.	-0.18	-1942.20	971.01	90.00
3	10	-4627.96	-0.23	0.	-0.23	-4627.96	2313.87	90.00
4	10	-7313.93	-0.15	0.	-0.15	-7313.93	3656.89	90.00
5	10	-0.00	-0.00	0.	-0.00	-0.00	0.00	90.00
6	10	7313.92	0.15	0.	7313.92	0.15	3656.88	0.
7	10	4627.96	0.23	0.	4627.96	0.23	2313.87	0.
8	10	1942.21	0.18	0.	1942.21	0.18	971.01	0.
9	10	-743.32	0.	0.	-0.	-743.32	371.66	90.00

BOTT STRESS 360 ELEMENT MODEL TEMPERATURE DISTRIBUTION A100

ROW	COL	XX-STRESS PSI	YY-STRESS PSI	XY-STRESS PSI	MAX-STRESS PSI	MIN-STRESS PSI	SHEAR STRESS PSI	DIRECTION DEG
1	1	0.	0.	0.	0.	0.	0.	ISOTROPIC POINT
2	1	0.	449.90	0.	449.90	0.	224.95	90.00
3	1	0.	708.90	0.	708.90	0.	354.45	90.00
4	1	0.	854.16	0.	854.16	0.	427.08	90.00
5	1	0.	932.88	0.	932.88	0.	466.44	90.00
6	1	0.	973.41	0.	973.41	0.	486.71	90.00
7	1	0.	992.16	0.	992.16	0.	496.08	90.00
8	1	0.	997.54	0.	997.54	0.	498.77	90.00
9	1	0.	992.16	0.	992.16	0.	496.08	90.00
10	1	0.	973.41	0.	973.41	0.	486.71	90.00
11	1	0.	932.88	0.	932.88	0.	466.44	90.00
12	1	0.	854.16	0.	854.16	0.	427.08	90.00
13	1	0.	708.90	0.	708.90	0.	354.45	90.00
14	1	0.	449.90	0.	449.90	0.	224.95	90.00
15	1	0.	0.	0.	0.	0.	0.	ISOTROPIC POINT
1	2	-1421.16	0.	-689.87	279.79	-1700.96	990.37	-67.92
2	2	-859.04	-62.45	-497.90	176.86	-1098.35	637.61	-64.33
3	2	-511.83	-45.03	-352.03	143.95	-700.81	422.38	-61.77
4	2	-299.46	2.67	-242.63	137.42	-434.21	285.81	-60.95
5	2	-171.80	54.50	-160.38	137.63	-254.93	196.28	-62.60
6	2	-98.07	97.26	-97.09	137.30	-138.12	137.71	-67.58
7	2	-60.12	124.66	-45.69	135.34	-70.80	103.07	-76.84
8	2	-48.45	134.04	-0.00	134.04	-48.45	91.25	-90.00
9	2	-60.12	124.66	45.69	135.34	-70.80	103.07	76.84
10	2	-98.07	97.26	97.09	137.30	-138.12	137.71	67.58
11	2	-171.80	54.50	160.38	137.63	-254.93	196.28	62.60
12	2	-299.46	2.67	242.63	137.42	-434.21	285.81	60.95
13	2	-511.83	-45.03	352.03	143.94	-700.81	422.38	61.77
14	2	-859.04	-62.45	497.90	176.86	-1098.35	637.61	64.33
15	2	-1421.16	0.	689.87	279.79	-1700.96	990.38	67.92
1	3	-1304.38	0.	-337.02	81.93	-1386.31	734.12	-76.34
2	3	-999.24	-78.18	-366.17	49.65	-1127.07	588.36	-70.76
3	3	-751.14	-130.60	-338.97	18.66	-900.40	459.53	-66.23
4	3	-561.72	-160.71	-283.83	-13.71	-708.72	347.50	-62.62
5	3	-425.25	-175.20	-216.44	-50.27	-550.18	249.95	-60.01
6	3	-334.31	-180.56	-144.79	-93.51	-421.37	163.93	-58.98
7	3	-282.51	-181.77	-72.33	-144.00	-320.27	88.14	-62.43
8	3	-265.71	-181.83	0.00	-181.83	-265.71	41.94	90.00
9	3	-282.51	-181.77	72.33	-144.00	-320.27	88.14	62.43
10	3	-334.31	-180.56	144.79	-93.51	-421.37	163.93	58.98
11	3	-425.25	-175.20	216.44	-50.27	-550.18	249.95	60.01
12	3	-561.72	-160.71	283.83	-13.71	-708.72	347.50	62.62
13	3	-751.14	-130.60	338.97	18.66	-900.40	459.53	66.23
14	3	-999.25	-78.18	366.17	49.65	-1127.08	588.36	70.76
15	3	-1304.38	0.	337.02	81.93	-1386.31	734.12	76.34
1	4	-1022.78	0.	-149.21	21.32	-1044.10	532.71	-81.87
2	4	-907.58	-44.40	-201.10	0.15	-952.13	476.14	-77.51
3	4	-789.68	-89.50	-213.80	-29.38	-849.81	410.21	-74.29
4	4	-683.37	-128.77	-197.90	-65.39	-746.75	340.68	-72.24
5	4	-596.55	-159.47	-162.39	-105.74	-650.28	272.27	-71.69
6	4	-533.09	-180.98	-114.28	-147.15	-566.93	209.89	-73.51
7	4	-494.67	-193.59	-58.82	-182.51	-505.75	161.62	-79.33
8	4	-481.82	-197.73	-0.00	-197.73	-481.82	142.04	-90.00
9	4	-494.67	-193.59	58.82	-182.51	-505.75	161.62	79.33
10	4	-533.09	-180.98	114.28	-147.15	-566.93	209.89	73.51
11	4	-596.55	-159.47	162.39	-105.74	-650.27	272.27	71.69
12	4	-683.37	-128.77	197.90	-65.39	-746.75	340.68	72.24
13	4	-789.69	-89.50	213.80	-29.38	-849.81	410.22	74.29
14	4	-907.58	-44.40	201.10	0.15	-952.13	476.14	77.51
15	4	-1022.78	0.	149.21	21.32	-1044.11	532.71	81.87
1	5	-858.81	0.	-66.35	5.10	-863.91	434.50	-85.61
2	5	-822.18	-22.37	-97.18	-10.73	-833.82	411.55	-83.17
3	5	-775.77	-49.06	-110.60	-32.60	-792.22	379.81	-81.54
4	5	-727.96	-75.60	-108.12	-58.15	-745.41	343.63	-80.83
5	5	-685.12	-98.79	-92.53	-84.53	-699.38	307.42	-81.24
6	5	-651.72	-116.53	-67.09	-108.25	-660.00	275.88	-82.96
7	5	-630.62	-127.59	-35.15	-125.15	-633.06	253.96	-86.02
8	5	-623.43	-131.34	-0.00	-131.34	-623.43	246.04	-90.00
9	5	-630.62	-127.59	35.15	-125.15	-633.07	253.96	86.02
10	5	-651.72	-116.53	67.09	-108.25	-660.00	275.88	82.96
11	5	-685.12	-98.79	92.53	-84.53	-699.38	307.42	81.24
12	5	-727.96	-75.60	108.12	-58.15	-745.41	343.63	80.83
13	5	-775.77	-49.06	110.60	-32.60	-792.23	379.81	81.54
14	5	-822.19	-22.37	97.18	-10.73	-833.82	411.55	83.17
15	5	-858.81	0.	66.35	5.10	-863.91	434.50	85.61

BOTT STRESS 360 ELEMENT MODEL TEMPERATURE DISTRIBUTION A100

ROW	COL	XX-STRESS PSI	YY-STRESS PSI	XY-STRESS PSI	MAX-STRESS PSI	MIN-STRESS PSI	SHEAR STRESS PSI	DIRECTION DEG
1	6	-784.65	0.	-28.25	1.02	-785.67	393.34	-87.94
2	6	-775.76	-10.54	-42.41	-8.19	-778.10	384.95	-86.84
3	6	-760.43	-23.96	-49.98	-20.59	-763.81	371.61	-86.14
4	6	-742.33	-38.13	-50.45	-34.54	-745.93	355.70	-85.92
5	6	-724.72	-51.14	-44.31	-48.24	-727.62	339.69	-86.25
6	6	-710.23	-61.50	-32.74	-59.85	-711.88	326.01	-87.12
7	6	-700.78	-68.14	-17.35	-67.66	-701.25	316.80	-88.43
8	6	-697.50	-70.42	-0.00	-70.42	-697.50	313.54	-90.00
9	6	-700.78	-68.14	17.35	-67.66	-701.25	316.80	88.43
10	6	-710.23	-61.50	32.74	-59.85	-711.88	326.01	87.12
11	6	-724.72	-51.14	44.31	-48.24	-727.63	339.69	86.25
12	6	-742.34	-38.13	50.45	-34.54	-745.93	355.70	85.92
13	6	-760.43	-23.96	49.98	-20.59	-763.81	371.61	86.14
14	6	-775.76	-10.54	42.41	-8.19	-778.10	384.95	86.84
15	6	-784.65	0.	28.25	1.02	-785.67	393.34	87.94
1	7	-755.74	0.	-10.99	0.16	-755.90	378.03	-89.17
2	7	-755.34	-4.55	-16.54	-4.19	-755.70	375.76	-88.74
3	7	-751.75	-10.53	-19.92	-9.99	-752.29	371.15	-88.46
4	7	-746.32	-17.03	-20.57	-16.45	-746.90	365.22	-88.39
5	7	-740.42	-23.18	-18.42	-22.71	-740.89	359.09	-88.53
6	7	-735.25	-28.19	-13.80	-27.92	-735.51	353.80	-88.88
7	7	-731.75	-31.44	-7.38	-31.36	-731.83	350.23	-89.40
8	7	-730.52	-32.57	0.00	-32.57	-730.52	348.97	90.00
9	7	-731.75	-31.44	7.38	-31.36	-731.83	350.23	89.40
10	7	-735.25	-28.19	13.80	-27.92	-735.52	353.80	88.88
11	7	-740.42	-23.18	18.42	-22.71	-740.90	359.09	88.53
12	7	-746.33	-17.03	20.57	-16.45	-746.91	365.23	88.39
13	7	-751.76	-10.53	19.92	-9.99	-752.29	371.15	88.46
14	7	-755.34	-4.55	16.54	-4.19	-755.71	375.76	88.74
15	7	-755.74	0.	10.99	0.16	-755.90	378.03	89.17
1	8	-746.18	0.	-3.75	0.02	-746.20	373.11	-89.71
2	8	-747.70	-1.75	-5.58	-1.70	-747.74	373.02	-89.57
3	8	-747.87	-4.08	-6.86	-4.01	-747.94	371.96	-89.47
4	8	-747.09	-6.68	-7.25	-6.60	-747.16	370.28	-89.44
5	8	-745.82	-9.19	-6.61	-9.13	-745.88	368.38	-89.49
6	8	-744.52	-11.27	-5.02	-11.23	-744.55	366.66	-89.61
7	8	-743.58	-12.63	-2.71	-12.62	-743.59	365.48	-89.79
8	8	-743.23	-13.11	0.00	-13.11	-743.23	365.06	90.00
9	8	-743.58	-12.64	2.71	-12.63	-743.59	365.48	89.79
10	8	-744.52	-11.27	5.02	-11.23	-744.56	366.66	89.61
11	8	-745.82	-9.19	6.61	-9.13	-745.88	368.38	89.49
12	8	-747.09	-6.68	7.25	-6.60	-747.16	370.28	89.44
13	8	-747.87	-4.08	6.86	-4.01	-747.94	371.96	89.47
14	8	-747.70	-1.75	5.58	-1.70	-747.74	373.02	89.57
15	8	-746.18	0.	3.75	0.02	-746.20	373.11	89.71
1	9	-743.71	0.	-1.03	0.00	-743.71	371.85	-89.92
2	9	-745.32	-0.58	-1.50	-0.57	-745.33	372.38	-89.88
3	9	-746.42	-1.36	-1.89	-1.36	-746.42	372.53	-89.85
4	9	-747.05	-2.28	-2.05	-2.27	-747.06	372.39	-89.84
5	9	-747.33	-3.18	-1.91	-3.18	-747.34	372.08	-89.85
6	9	-747.40	-3.95	-1.47	-3.95	-747.40	371.73	-89.89
7	9	-747.38	-4.46	-0.80	-4.46	-747.38	371.46	-89.94
8	9	-747.36	-4.64	0.00	-4.64	-747.36	371.36	90.00
9	9	-747.38	-4.46	0.80	-4.46	-747.38	371.46	89.94
10	9	-747.40	-3.95	1.47	-3.95	-747.40	371.73	89.89
11	9	-747.33	-3.18	1.91	-3.17	-747.34	372.08	89.85
12	9	-747.05	-2.27	2.05	-2.27	-747.06	372.40	89.84
13	9	-746.42	-1.36	1.89	-1.36	-746.43	372.53	89.85
14	9	-745.32	-0.58	1.50	-0.57	-745.33	372.38	89.88
15	9	-743.71	0.	1.03	0.00	-743.71	371.86	89.92
1	10	-743.32	0.	0.	-0.	-743.32	371.66	90.00
2	10	-744.84	-0.27	0.	-0.27	-744.84	372.29	90.00
3	10	-746.07	-0.64	0.	-0.64	-746.07	372.71	90.00
4	10	-746.99	-1.09	0.	-1.09	-746.99	372.95	90.00
5	10	-747.61	-1.56	0.	-1.56	-747.61	373.02	90.00
6	10	-747.98	-1.97	0.	-1.97	-747.98	373.01	90.00
7	10	-748.19	-2.24	0.	-2.24	-748.19	372.97	90.00
8	10	-748.24	-2.34	0.	-2.34	-748.24	372.95	90.00
9	10	-748.19	-2.24	0.	-2.24	-748.19	372.97	90.00
10	10	-747.98	-1.97	0.	-1.97	-747.98	373.01	90.00
11	10	-747.61	-1.56	0.	-1.56	-747.61	373.02	90.00
12	10	-746.99	-1.09	0.	-1.09	-746.99	372.95	90.00
13	10	-746.07	-0.64	0.	-0.64	-746.07	372.72	90.00
14	10	-744.84	-0.27	0.	-0.27	-744.84	372.29	90.00
15	10	-743.32	0.	0.	-0.	-743.32	371.66	90.00

PORT STRESS 360 ELEMENT MODEL TEMPERATURE DISTRIBUTION A100

ROW	COL	XX-STRESS PSI	YY-STRESS PSI	XY-STRESS PSI	MAX-STRESS PSI	MIN-STRESS PSI	SHEAR STRESS PSI	DIRECTION DEG
1	1	0.	0.	0.	0.	0.	0.	ISOTROPIC POINT
2	1	0.	-765.71	0.	-0.	-765.71	382.86	0.
3	1	0.	-1377.53	0.	-0.	-1377.53	688.76	0.
4	1	0.	-1336.10	0.	-0.	-1336.10	668.05	0.
5	1	0.	-0.00	0.	-0.	-0.00	0.00	0.
6	1	0.	1336.09	0.	1336.09	0.	668.05	90.00
7	1	0.	1377.53	0.	1377.53	0.	688.76	90.00
8	1	0.	765.71	0.	765.71	0.	382.86	90.00
9	1	0.	0.	0.	0.	0.	0.	ISOTROPIC POINT
1	2	-1421.16	0.	689.87	279.79	-1700.96	990.38	67.92
2	2	692.55	233.34	685.82	1186.18	-260.29	723.24	35.75
3	2	2939.61	463.10	233.39	2961.41	441.30	1260.06	5.34
4	2	5825.98	492.53	-685.82	5912.75	405.75	2753.50	-7.21
5	2	0.00	0.00	-1265.35	1265.35	-1265.35	1265.35	-45.00
6	2	-5825.97	-492.53	-685.82	-405.75	-5912.75	2753.50	-82.79
7	2	-2939.61	-463.10	233.39	-441.30	-2961.41	1260.06	84.66
8	2	-692.55	-233.34	685.82	260.29	-1186.18	723.23	54.26
9	2	1421.16	0.	689.87	1700.96	-279.79	990.38	22.08
1	3	-1304.38	0.	337.02	81.93	-1386.31	734.12	76.34
2	3	1352.95	96.49	221.46	1390.84	58.60	666.12	9.71
3	3	4076.19	156.05	15.85	4076.25	155.99	1960.13	0.23
4	3	6954.37	127.36	-221.46	6961.54	120.18	3420.68	-1.86
5	3	0.00	-0.00	-335.53	335.53	-335.53	335.53	-45.00
6	3	-6954.36	-127.36	-221.46	-120.18	-6961.54	3420.68	-88.14
7	3	-4076.19	-156.05	15.85	-155.99	-4076.25	1960.13	89.77
8	3	-1352.95	-96.49	221.46	-58.61	-1390.84	666.12	80.29
9	3	1304.38	0.	337.02	1386.31	-81.93	734.12	13.66
1	4	-1022.78	0.	149.21	21.32	-1044.11	532.71	81.87
2	4	1680.93	31.33	72.03	1684.07	28.19	827.94	2.50
3	4	4418.47	43.18	-6.97	4418.48	43.17	2187.65	-0.09
4	4	7194.82	30.90	-72.03	7195.54	30.18	3582.68	-0.58
5	4	0.00	0.00	-98.14	98.14	-98.14	98.14	-45.00
6	4	-7194.81	-30.90	-72.03	-30.18	-7195.54	3582.68	-89.42
7	4	-4418.47	-43.18	-6.97	-43.17	-4418.48	2187.65	-89.91
8	4	-1680.93	-31.33	72.03	-28.19	-1684.07	827.94	87.50
9	4	1022.77	0.	149.21	1044.10	-21.32	532.71	8.13
1	5	-858.81	0.	66.35	5.10	-863.91	434.50	85.61
2	5	1833.59	12.39	28.15	1834.03	11.95	911.04	0.89
3	5	4543.57	15.32	-4.96	4543.57	15.32	2264.13	-0.06
4	5	7267.67	10.13	-28.15	7267.78	10.02	3628.88	-0.22
5	5	0.00	-0.00	-36.59	36.59	-36.59	36.59	-45.00
6	5	-7267.67	-10.13	-28.15	-10.02	-7267.78	3628.88	-89.78
7	5	-4543.57	-15.32	-4.96	-15.32	-4543.57	2264.13	-89.94
8	5	-1833.60	-12.39	28.15	-11.95	-1834.03	911.04	89.11
9	5	858.81	0.	66.35	863.90	-5.10	434.50	4.39
1	6	-784.65	0.	28.25	1.02	-785.67	393.34	87.94
2	6	1901.18	5.51	11.73	1901.25	5.44	947.91	0.35
3	6	4595.51	6.57	-2.29	4595.51	6.56	2294.47	-0.03
4	6	7296.08	4.22	-11.73	7296.10	4.20	3645.95	-0.09
5	6	0.00	-0.00	-15.07	15.07	-15.07	15.07	-45.00
6	6	-7296.08	-4.22	-11.73	-4.20	-7296.10	3645.95	-89.91
7	6	-4595.51	-6.57	-2.29	-6.57	-4595.51	2294.47	-89.97
8	6	-1901.18	-5.51	11.73	-5.44	-1901.26	947.91	89.65
9	6	784.65	0.	28.24	785.67	-1.02	393.34	2.06
1	7	-755.74	0.	10.99	0.16	-755.90	378.03	89.17
2	7	1928.68	2.40	4.67	1928.69	2.39	963.15	0.14
3	7	4616.81	2.85	-0.89	4616.81	2.85	2306.98	-0.01
4	7	7307.68	1.83	-4.67	7307.69	1.82	3652.93	-0.04
5	7	0.00	0.00	-6.00	6.01	-6.00	6.00	-45.00
6	7	-7307.68	-1.82	-4.67	-1.82	-7307.68	3652.93	-89.96
7	7	-4616.81	-2.85	-0.89	-2.85	-4616.81	2306.98	-89.99
8	7	-1928.68	-2.40	4.67	-2.39	-1928.69	963.15	89.86
9	7	755.74	0.	10.99	755.90	-0.16	378.03	0.83
1	8	-746.18	0.	3.75	0.02	-746.20	373.11	89.71
2	8	1938.59	0.96	1.67	1938.59	0.96	968.82	0.05
3	8	4624.81	1.15	-0.29	4624.81	1.15	2311.83	-0.00
4	8	7312.11	0.74	-1.67	7312.11	0.74	3655.69	-0.01
5	8	0.00	0.00	-2.16	2.16	-2.16	2.16	-44.99
6	8	-7312.11	-0.74	-1.67	-0.74	-7312.11	3655.69	-89.99
7	8	-4624.81	-1.15	-0.29	-1.15	-4624.81	2311.83	-90.00
8	8	-1938.59	-0.96	1.67	-0.96	-1938.60	968.82	89.95
9	8	746.18	0.	3.75	746.20	-0.02	373.11	0.29
1	9	-743.71	0.	1.03	0.00	-743.71	371.86	89.92
2	9	1941.60	0.35	0.49	1941.60	0.35	970.63	0.01
3	9	4627.40	0.42	-0.08	4627.40	0.42	2313.49	-0.00
4	9	7313.60	0.28	-0.49	7313.60	0.28	3656.66	-0.00
5	9	0.00	0.00	-0.64	0.64	-0.64	0.64	-44.93
6	9	-7313.59	-0.28	-0.49	-0.28	-7313.59	3656.66	-90.00
7	9	-4627.40	-0.42	-0.07	-0.42	-4627.40	2313.49	-90.00
8	9	-1941.61	-0.35	0.49	-0.35	-1941.61	970.63	89.99
9	9	743.71	0.	1.03	743.71	-0.00	371.86	0.08
1	10	-743.32	0.	0.	-0.	-743.32	371.66	90.00
2	10	1942.20	0.18	0.	1942.20	0.18	971.01	0.
3	10	4627.96	0.23	0.	4627.96	0.23	2313.87	0.
4	10	7313.92	0.15	0.	7313.92	0.15	3656.89	0.
5	10	0.00	-0.00	0.	0.00	-0.00	0.00	0.
6	10	-7313.92	-0.15	0.	-0.15	-7313.92	3656.88	90.00
7	10	-4627.96	-0.23	0.	-0.23	-4627.96	2313.87	90.00
8	10	-1942.21	-0.18	0.	-0.18	-1942.21	971.01	90.00
9	10	743.32	0.	0.	743.32	0.	371.66	0.

APPENDIX B - TABLULAR EXPERIMENTAL DATA AND RESULTS PRESENTED GRAPHICALLY IN FIGS. 14, 17, AND 18.

TABLE B-1. MODEL MIDSHIP SECTION GEOMETRY DATA FOR FIG. 14.

ELEMENT NO.	ELEMENT AREA SQ.-IN.	X CO-ORDINATE FT.	Y CO-ORDINATE FT.
1	0.3343	+1.2040	+0.7958
2	0.3343	-1.2040	+0.7958
3	0.4069	+0.9991	+0.7800
4	0.4069	-0.9991	+0.7800
5	0.4110	+0.7500	+0.7800
6	0.4110	-0.7500	+0.7800
7	0.4110	+0.5000	+0.7800
8	0.4110	-0.5000	+0.7800
9	0.4110	+0.2500	+0.7800
10	0.4110	-0.2500	+0.7800
11	0.4110	+0.0000	+0.7800
12	0.3535	+1.2440	+0.7542
13	0.3535	-1.2440	+0.7542
14	0.4343	+1.2440	+0.5150
15	0.4343	-1.2440	+0.5150
16	0.4110	+1.2440	+0.2575
17	0.4110	-1.2440	+0.2575
18	0.4631	+1.2440	-0.0083
19	0.4631	-1.2440	-0.0083
20	0.1192	+1.2440	-0.1858
21	0.1192	-1.2440	-0.1858
22	0.0685	+1.2440	-0.2425
23	0.0685	-1.2440	-0.2425
24	0.0685	+1.2440	-0.2842
25	0.0685	-1.2440	-0.2842
26	0.1192	+1.2440	-0.3417
27	0.1192	-1.2440	-0.3417
28	0.3261	+1.2440	-0.4767
29	0.3261	-1.2440	-0.4767
30	0.2809	+1.2440	-0.6617
31	0.2809	-1.2440	-0.6617
32	0.1836	+1.2440	-0.8025
33	0.1836	-1.2440	-0.8025
34	0.3357	+1.1250	-0.8408
35	0.3357	-1.1250	-0.8408
36	0.7562	+0.7925	-0.8408
37	0.7562	-0.7925	-0.8408
38	0.6165	+0.3750	-0.8408
39	0.6165	-0.3750	-0.8408
40	0.6165	+0.0000	-0.8408

TABLE B-2 - TEMPERATURE CONVERSION TABLE.

TEMPERATURE READING UNITS	TEMPERATURE DEG-F
109	30.0
139	39.0
170	47.5
204	57.0
229	64.0
261	73.0
286	80.0
315	88.0
331	92.0
350	97.0
371	103.0
392	108.5
410	113.0
433	119.0
448	123.0
467	128.0
490	134.0
514	140.0
530	144.0
549	149.0
571	154.5
593	160.0
612	165.0
633	170.0
653	175.0
673	180.0
693	185.0
714	190.0
775	205.0
797	210.0

TABLE B-3 -APPARENT STRAIN CALIBRATION TABLE - STRAIN GAGE LOT A5-L-1.

TEMPERATURE DEG-F	APPARENT STRAIN $IN/IN \times 10^{-6}$
50.0	-53.0
52.5	-47.5
55.0	-42.0
57.5	-37.3
60.0	-32.5
62.5	-28.3
65.0	-24.0
67.5	-21.0
70.0	-17.3
72.5	-14.0
75.0	-11.5
77.5	-9.0
80.0	-7.0
82.5	-5.0
85.0	-3.5
87.5	-2.3
90.0	-1.5
92.5	-1.0
95.0	-0.5
97.5	-0.5
100.0	-1.0
102.5	-1.5
105.5	-2.5
107.5	-3.5
110.0	-4.5
112.5	-6.0
115.0	-7.5
117.5	-9.5
120.0	-11.3
122.5	-13.5
125.0	-16.0
127.5	-18.5
130.0	-21.0
132.5	-24.0
135.0	-27.0
137.5	-30.0
140.0	-33.5
142.5	-37.0
145.0	-40.5
147.5	-44.5
150.0	-48.5
152.5	-52.5
155.0	-57.0
157.5	-61.0
160.0	-65.5
162.5	-70.0
165.0	-74.5
167.5	-79.5
170.0	-84.0

TABLE B-4 - DATA FOR FIGURE 17.

ELEMENT	TEMPERATURE READINGS		STRAIN READINGS				TEMPERATURE CHANGE	COMPUTED STRESS PSI		
			LONGITUDINAL		TRANSVERSE			FROM STRAIN READINGS		FROM TEMPERATURE CHANGE
NO.	INITIAL	FINAL	INITIAL	FINAL	INITIAL	FINAL	DEG-F	LONGITUDINAL	TRANSVERSE	LONGITUDINAL
1	196	571	508	530	503	479	99.7	1060	-15	770
2	196	535	508	538	510	525	90.6	1050	700	1090
3	196	579	507	498	506	482	101.7	190	-160	47
4	195	555	503	490	502	490	96.0	-280	-250	-65
5	195	586	507	476	506	473	103.8	-510	-560	-530
6	195	568	504	464	503	505	99.3	-800	180	-570
7	195	590	503	454	510	490	104.8	-900	-220	-890
8	195	574	507	450	505	471	100.8	-1570	-1030	-720
9	195	590	506	461	507	474	104.8	-890	-610	-1050
10	195	578	504	444	502	473	101.8	-1560	-830	-760
11	195	586	509	456	507	468	103.8	-1280	-950	-1000
12	196	562	501	527	504	486	97.5	1080	50	730
13	196	516	502	564	502	515	85.7	1790	640	1530
14	196	533	506	500	503	530	90.0	-46	730	-720
15	196	469	503	544	508	619	73.8	1390	3030	980
16	196	490	500	461	504	521	79.2	-1810	-500	-1720
17	197	421	498	536	503	534	60.8	110	-50	410
18	197	421	504	500	507	536	60.8	-1270	-500	-1300
19	197	357	501	553	503	528	44.0	210	-430	510
20	197	300	502	625	503	506	28.8	2460	-350	2940
21	198	293	502	578	501	511	26.6	1070	-480	1820
22	198	274	501	661	504	522	21.3	4060	730	3750
23	198	277	500	602	504	527	22.2	2180	330	2000
24	198	256	509	670	510	495	16.3	4010	-110	4240
25	198	260	497	602	503	512	17.4	2350	100	2460
26	198	244	502	661	508	486	12.9	4080	-160	4220
27	198	248	505	612	506	507	14.0	2530	45	2430
28	198	219	504	631	509	484	5.9	3450	-110	3960
29	198	220	500	582	501	492	6.2	2110	-20	2330
30	198	212	503	573	495	483	3.9	1860	-60	2080
31	199	212	502	532	509	509	3.6	690	-15	570
32	199	210	510	524	499	503	3.1	250	15	500
33	199	210	505	483	507	524	3.1	-800	110	-1060
34	199	210	503	497	506	513	3.1	-370	-70	-45
35	199	210	508	471	505	519	3.1	-1320	-125	-1460
36	199	211	500	486	503	511	3.4	-650	-130	-310
37	198	211	508	477	716	730	3.6	-1170	-115	-1350
38	199	211	506	487	506	518	3.4	-775	-50	-580
39	199	211	502	476	502	519	3.4	-960	50	-1050
40	199	211	503	492	499	530	3.4	-340	640	-810

TABLE B-5 - DATA FOR FIGURE 18.

ELEMENT	TEMPERATURE READINGS		STRAIN READINGS				TEMPERATURE CHANGE	COMPUTED STRESS PSI		
			LONGITUDINAL		TRANSVERSE			FROM STRAIN READINGS		FROM TEMPERATURE CHANGE
NO.	INITIAL	FINAL	INITIAL	FINAL	INITIAL	FINAL	DEG-F	LONGITUDINAL	TRANSVERSE	LONGITUDINAL
1	263	501	498	476	464	450	63.2	-170	17	-87
2	263	407	390	445	385	389	38.7	1530	340	1530
3	265	499	465	443	477	459	62.1	-210	-115	-260
4	266	452	467	448	478	474	49.7	-530	-180	-510
5	267	498	476	449	469	450	61.3	-370	-180	-440
6	268	477	509	454	556	561	55.6	-1320	86	-1360
7	269	495	439	409	470	456	60.0	-440	-60	-520
8	269	486	450	389	470	456	57.7	-1560	-460	-1430
9	270	494	441	410	477	457	59.5	-520	-270	-760
10	270	489	448	395	504	487	58.2	-1280	-430	-1190
11	270	491	462	423	475	454	58.7	-830	-410	-950
12	260	501	471	444	486	475	64.0	-340	34	-480
13	260	377	498	600	496	495	31.9	2830	420	2550
14	253	481	481	433	485	507	60.9	-1080	560	-1490
15	254	332	470	575	465	487	21.2	3000	1050	3060
16	244	443	471	417	470	487	53.4	-1900	-240	-1750
17	245	303	459	538	473	472	16.2	1900	28	2300
18	232	373	472	476	527	551	38.7	-580	-115	-620
19	234	274	449	504	442	442	11.2	1220	-68	1490
20	221	271	541	657	528	515	14.0	2870	-150	3130
21	222	243	545	588	525	522	5.9	1010	-70	1340
22	221	254	567	699	534	534	9.3	3730	640	3690
23	221	238	525	571	508	513	4.8	1240	275	1170
24	217	243	490	626	628	621	7.3	3900	550	3800
25	217	231	510	553	484	483	3.9	1110	81	1060
26	217	237	555	688	474	455	5.6	3780	220	3750
27	217	227	525	563	470	471	2.8	1050	180	890
28	212	223	606	714	494	475	3.1	3120	140	3330
29	211	219	530	538	455	463	2.2	165	165	87
30	209	218	510	589	518	506	2.5	2270	140	2180
31	209	215	527	503	560	575	1.7	-780	135	-1080
32	208	215	503	550	503	499	2.0	1340	140	1320
33	208	214	469	415	492	517	1.7	-1660	190	-2040
34	208	214	454	492	473	472	1.7	1090	180	950
35	208	214	471	416	479	503	1.7	-1710	145	-2140
36	208	214	512	527	474	476	1.7	370	67	490
37	207	214	609	563	878	895	2.0	-1500	-23	-1750
38	207	214	457	460	427	435	2.0	14	130	-140
39	207	214	467	440	469	489	2.0	-850	250	-1170
40	208	214	676	668	720	745	1.7	-170	600	-595

APPENDIX C

Calibration and Instrumentation

Strain Gage Calibrations

Two basic calibration tests were performed on the electrical resistance strain gages. The first test made was that of determining the effective gage factor and gage factor temperature correction, the second test was that of determining the apparent strain curve for the strain gages.

The installation of the strain gage into an electrical network always causes a desensitization of the gage, and hence the need for a careful determination of the effective gage factor arises. This determination was carried out by placing gages on a calibrated bar in a tensile testing machine, and observing the strain gage output versus the known applied strains. The effective gage factor thus found was 2.00. The strain gages used in this investigation had a manufacturer's gage factor of 2.01. It was further determined that within the temperature range of 45 F to 180 F that no measurable change in the effective gage factor occurred.

When an electrical strain gage is mounted on a stress free specimen and subjected to temperature excursions it is observed that in general the strain reading is a nonlinear function of the temperature. This effect makes necessary a careful temperature calibration of the strain gages. To make this test, gages chosen at random from those received from the manufacturer were mounted on test coupons cut from the steel sheet from which the model was fabricated. These small test coupons were then placed in a small test oven to permit accurately controlled temperature excursions. Simultaneous temperature and strain gage measurements were then made to obtain the apparent strain curve. The reproducibility of this curve from different gages was within the least count of the measuring instrument, which was $\pm$ 1 micro-inch/inch. For computational work this experimental curve was reduced to a table which is given in Appendix B.

Material Tests

Routine tensile tests were carried out on steel specimens cut from the steel sheet from which the model was fabricated. The elastic modulus was determined to be 30.0×10^6 psi, and the Poisson's ratio was found to be 0.28.

Specimens cut from the length and width directions of the steel sheet were tested to determine if any measurable anisotropic effects were present. To within the accuracy of the measuring instruments, the specimens from the two perpendicular directions yielded the same elastic constants.

Bolt Slip Test

During the early design phase of this investigation it was necessary to experimentally check the behavior of the proposed bolted joint connection between the sides of the model and the deck. A test jig was fabricated which permitted the testing of bolted connection in a universal testing machine. Tests made with this jig indicated the joint had adequate strength and that it showed no indication of slipping until loads well in excess of design loads were applied.

SHIP HULL RESEARCH COMMITTEE
(Successor to Committee on Ship Structural Design)

Division of Engineering & Industrial Research
National Academy of Sciences–National Research Council

Chairman:

RADM A. G. Mumma, USN (Ret.)
Vice President
Worthington Corporation

Members:

Mr. Hollinshead de Luce
Assistant to Vice President
Bethlehem Steel Co. Shipbuilding Div.

Professor J. Harvey Evans
Professor of Naval Architecture
Massachusetts Institute of Technology

Mr. M. G. Forrest
Vice President — Naval Architecture
Gibbs & Cox, Inc.

Mr. James Goodrich
General Manager
Todd Shipyards, Los Angeles Div.

Professor N. J. Hoff
Head, Dept. of Aeronautics & Astronautics
Stanford University

Mr. M. W. Lightner
Vice President, Applied Research
U. S. Steel Corporation

Arthur R. Lytle
Director

R. W. Rumke
Executive Secretary